


METHODS AND APPROACHES

A high-throughput fluorescence lifetime-based assay to detect binding of myosin-binding protein C to F-actin

Thomas A. Bunch, Victoria C. Lepak, Kellan M. Bortz, and Brett A. Colson 

Binding properties of actin-binding proteins are typically evaluated by cosedimentation assays. However, this method is time-consuming, involves multiple steps, and has a limited throughput. These shortcomings preclude its use in screening for drugs that modulate actin-binding proteins relevant to human disease. To develop a simple, quantitative, and scalable F-actin-binding assay, we attached fluorescent probes to actin’s Cys-374 and assessed changes in fluorescence lifetime upon binding to the N-terminal region (domains C0–C2) of human cardiac myosin-binding protein C (cMyBP-C). The lifetime of all five probes tested decreased upon incubation with cMyBP-C C0–C2, as measured by time-resolved fluorescence (TR-F), with IAEDANS being the most sensitive probe that yielded the smallest errors. The TR-F assay was compared with cosedimentation to evaluate in vitro changes in binding to actin and actin–tropomyosin arising from cMyBP-C mutations associated with hypertrophic cardiomyopathy (HCM) and tropomyosin binding. Lifetime changes of labeled actin with added C0–C2 were consistent with cosedimentation results. The HCM mutation L352P was confirmed to enhance actin binding, whereas PKA phosphorylation reduced binding. The HCM mutation R282W, predicted to disrupt a PKA recognition sequence, led to deficits in C0–C2 phosphorylation and altered binding. Lastly, C0–C2 binding was found to be enhanced by tropomyosin and binding capacity to be altered by mutations in a tropomyosin-binding region. These findings suggest that the TR-F assay is suitable for rapidly and accurately determining quantitative binding and for screening physiological conditions and compounds that affect cMyBP-C binding to F-actin for therapeutic discovery.

Introduction

Actin-binding proteins (ABPs) play key roles in skeletal and cardiac muscle (dos Remedios and Thomas, 2001). In cardiac muscle, ABPs are involved in the assembly, organization, and maintenance of the sarcomeres for normal contraction. Examples of muscle ABPs include the motor protein myosin, which interacts with actin to produce force; the tropomyosin (Tm)–troponin complex, which regulates actin’s exposure to myosin to regulate force production; and nebulin and leiomodin/tropomodulin proteins, which regulate thin filament length. Additionally, a thick filament-associated sarcomeric protein, cardiac myosin-binding protein C (cMyBP-C), is an ABP that is anchored to myosin and titin at its C-terminal end and extends toward actin at its N terminus to modulate the strength and speed of myosin cross-bridge cycling (for review, see van Dijk et al., 2014; Moss et al., 2015). Mutations in cMyBP-C, myosin, Tm, and troponin have been shown to cause cardiomyopathy in humans (Ingles et al., 2019). Mutations in cMyBP-C are a leading cause of

hypertrophic cardiomyopathy (HCM; Ingles et al., 2019), including truncation mutations that lead to haploinsufficiency and missense mutations that alter binding function. cMyBP-C function is regulated by PKA-mediated phosphorylation, which reduces N-terminal cMyBP-C binding to actin (Shaffer et al., 2009) and myosin (Gruen et al., 1999). Decreases in phosphorylation of cMyBP-C have been observed in heart failure of human patients and animal models (El-Armouche et al., 2007), and phosphorylation is cardioprotective in mouse models (Sadayappan et al., 2006). Thus, increases in phosphorylation or drugs that mimic phosphorylation of cMyBP-C could be a therapeutic option for heart failure. As there are no therapies targeting cMyBP-C or its interactions with actin (or myosin), developing screening technology to identify drugs that modulate actin binding and/or mimic phosphorylation of cMyBP-C is the focus of this work.

The binding of filamentous actin (F-actin) to ABPs, including cMyBP-C, can be studied using a wide variety of technologies,

Department of Cellular and Molecular Medicine, University of Arizona, Tucson, AZ.

Correspondence to Brett A. Colson: bcolson@arizona.edu

This work is part of a special collection on myofilament function and disease.

© 2021 Bunch et al. This article is distributed under the terms of an Attribution–Noncommercial–Share Alike–No Mirror Sites license for the first six months after the publication date (see <http://www.rupress.org/terms/>). After six months it is available under a Creative Commons License (Attribution–Noncommercial–Share Alike 4.0 International license, as described at <https://creativecommons.org/licenses/by-nc-sa/4.0/>).

including cosedimentation, affinity chromatography, electron microscopy, immunofluorescence imaging, and transient phosphorescence anisotropy. These methods are useful for studying details of ABP-actin interactions but are labor intensive and not scalable to the degree required for use in screening libraries of chemicals for potential therapeutic drugs. They also limit the number of variables that can be tested in the binding assay.

The development of multiwell plate readers with the capacity to precisely measure fluorescence lifetimes (time-resolved fluorescence; TR-F) in the nanosecond time scale gives rise to the potential of using changes in lifetime to monitor binding of a labeled protein, such as actin, to an unlabeled binding partner. The lifetime of a fluorescent molecule (e.g., 5-(((2-iodoacetyl)amino)ethyl)amino)naphthalene-1-sulfonic acid; IAEDANS) is the time it remains in the excited state before returning to the ground state. Following an excitation pulse (e.g., from a microchip laser or LED source), excited molecules return to the ground state over a few nanoseconds. TR-F is capable of observing the fluorescence emission levels over this time. In addition to radiative decay, the emission of photons as a portion of the excited fluorescent molecules return to the ground state, excited molecules can return to the ground state by nonradiative decay. Nonradiative decay occurs by energy transfer from a subpopulation of the excited molecules to the surrounding medium (buffer or, in the case of a probe attached to a protein, side chains of residues that are close to the probe). Changes in the environment of a fluorescent probe attached to actin due to interactions with another protein (an ABP) in the vicinity of that probe can increase or decrease the population of excited molecules that experience nonradiative decay. Changes in the nonradiative decay population influence the excited molecules available for radiative decay (fluorescence) and consequently can change the fluorescence lifetime. Changes in lifetime of a fluorescent probe on actin can therefore reflect binding of an ABP to actin if the interaction site is in close proximity to the label. Quantitatively, the degree of lifetime change reflects the number of actin-ABP complexes and can be used to generate binding curves. Changes in lifetime may be small (<10%), but the high precision with which they can be measured is such that even a 1% change can be reliably measured and used for screening chemical libraries for potential drugs that alter binding (Gruber et al., 2014) or testing of many physiological variables/biochemical conditions for mechanistic understanding. Changes in fluorescence indicative of actin binding, in a multiwell plate reader format, represent a potentially powerful screening tool to identify drugs that modulate ABPs and a high-throughput tool for scientific discovery.

To develop a simple, quantitative F-actin-binding assay in a 384-well plate format, we have screened potential fluorescent probes that when covalently attached to actin at position Cys-374 report binding, via change in lifetime. Actin's Cys-374 is naturally occurring and solvent exposed. This is in contrast to the other four cysteines in actin that are buried and not labeled by the reactive dyes under our labeling conditions (Otterbein et al., 2001; Bunch et al., 2019). All the probes we have tested showed a decrease in lifetime upon binding to cMyBP-C N-terminal domains C0 through C2 (C0-C2, whereas full-length cMyBP-C

includes domains C0-C10). IAEDANS-labeled F-actin, in the plate reader format, allowed for rapid and easy optimization of pH and ionic strength. Using our optimized conditions, we tested this system's ability to distinguish between binding mediated by phosphorylated and unphosphorylated cMyBP-C as well as HCM mutants or functional mutations in the Tm-binding region of cMyBP-C. The TR-F assay was able to detect the predicted binding changes to both actin and actin-Tm for variations in cMyBP-C. This finding suggests that it will be valuable in drug screening, assaying binding conditions of ABPs (e.g., PKA phosphorylation, buffer, pH, and Ca²⁺), and evaluation of mutations with unknown effects on actin binding. In our analysis of the HCM mutations in cMyBP-C, we also identified defects in phosphorylation and subsequent actin binding as a potential cause of the mutant phenotype in the cMyBP-C R282W mutation.

Materials and methods

Actin filament preparations

Actin was prepared from rabbit skeletal muscle by extracting acetone powder in cold water as described in Bunch et al. (2018). The day before actin-binding experiments (cosedimentation or TR-F), globular actin (G-actin) was polymerized by the addition of MgCl₂ to a final concentration of 3 mM for 1 h at 23°C. F-actin was collected by centrifugation at 4°C, 100,000 rpm (350,000 ×g) in a Beckman TLA-120.2 rotor, and the pellet was resuspended in MOPS actin-binding buffer (M-ABB; 100 mM KCl, 10 mM MOPS, pH 6.8, 2 mM MgCl₂, 0.2 mM CaCl₂, 0.2 mM ATP, 1 mM dithiothreitol [DTT], and 1 mM sodium azide). Any bundled actin was removed by centrifugation at 4°C, 15,000 rpm (21,000 ×g) for 10 min in an Eppendorf 5424R benchtop microfuge. The resulting F-actin at ~30 μM was stabilized by the addition of an equimolar amount of phalloidin. After 10 min at room temperature, unbound phalloidin was removed by centrifugation at 4°C, 15,000 rpm (21,000 ×g) for 10 min in an Eppendorf 5424R benchtop microfuge. F-actin was adjusted to 10 μM with M-ABB. For actin-Tm binding, Tm was added to a ratio of 3.5:1 (actin/Tm) and allowed to incubate overnight.

Actin labeling

For fluorescence experiments (TR-F), actin was labeled at Cys-374 with IAEDANS (Thermo Fisher Scientific). Labeling was done on F-actin. To 50 μM of G-actin in G-buffer (10 mM Tris, pH 7.5, 0.2 mM CaCl₂, and 0.2 mM ATP), Tris pH 7.5 was added to a final concentration of 20 mM and then polymerized by the addition of 3 M KCl (to a final concentration of 100 mM) and 0.5 M MgCl₂ (to a final concentration of 2 mM), followed by incubation at 23°C for 1 h. IAEDANS was added to a final concentration of 1 mM (from a 20 mM stock in dimethylformamide). Labeling was done for 3 h at 23°C and then overnight at 4°C. Labeling of actin with 2-(4'-(iodoacetamido)aniline)naphthalene-6-sulfonic acid (IAANS), N-((2-(iodoacetoxy)ethyl)-N-methyl)amino-7-nitrobenz-2-oxa-1,3-diazole (IANBD), and 7-diethylamino-3-(4'-maleimidylphenyl)-4-methylcoumarin (CPM) were done the same as IAEDANS, except with 250 μM IAANS and IANBD and 500 μM CPM for 1 h at 23°C. Labeling of actin

with fluorescein-5-maleimide (FMAL) was done as for IAEDANS, except labeling was for 5 h at 23°C. Labeling was terminated by the addition of DTT (to a final concentration of 5 mM). Labeled F-actin was collected by centrifugation for 30 min at 4°C, 100,000 rpm (350,000 $\times g$) in a Beckman TLA-120.2 rotor. The pellet was rinsed three times and then resuspended in labeling G-buffer (5 mM Tris pH 7.5, 0.2 mM CaCl₂, and 0.5 mM ATP). G-actin was clarified by centrifugation for 10 min, 4°C, 90,000 rpm (290,000 $\times g$) in a Beckman TLA-120.2 rotor. G-actin was then repolymerized by the addition of MgCl₂ to 3 mM and incubation at 23°C for 1 h. Labeled F-actin was collected by centrifugation for 30 min at 4°C, 100,000 rpm (350,000 $\times g$) in a Beckman TLA-120.2 rotor. The pellet was washed three times and then resuspended in M-ABB. Bundled actin was removed, and the labeled F-actin was stabilized with phalloidin and then complexed with Tm as described for unlabeled actin. Labeling efficiency was determined by measuring dye absorbance by UV-vis spectrophotometry, and protein concentration, measured with a Pierce BCA Protein Assay Kit (Thermo Fisher Scientific) using unmodified actin as a standard. The extent of labeling (dye/mol actin) was ~1.0 (IAEDANS), 1.0 (IAANS), 0.75 (IANBD), 0.65 (CPM), and 0.3 (FMAL).

Recombinant human Tm and Tm-actin filament preparations

The gene encoding human α -Tm was inserted into a pET3d vector and provided by J. C. Tardiff (University of Arizona, Tucson, AZ). Tm was expressed with two additional N-terminal amino acids (Ala-Ser) needed to ensure proper actin-binding and polymerization function, as bacterially expressed Tm is not otherwise functional due to lack of acetylation of the starting Met (Monteiro et al., 1994; McConnell et al., 2017). Protein production in *Escherichia coli* BL21(DE3)-competent cells (New England Biolabs) was done in ZYP broth (1% tryptone, 0.5% yeast extract, 0.5% glycerol, 0.05% glucose, and 0.2% lactose) and pelleted by centrifugation in a Beckman JA-10 rotor at 1,800 $\times g$ for 20 min at 4°C. Pellets were resuspended in double distilled H₂O, brought to 1 M saline with solid NaCl, and homogenized using the Emulsiflex C3 (Avestin). Cell debris of homogenized pellets was then pelleted by centrifugation in a Beckman JA-17 rotor at 28,950 $\times g$ for 10 min at 4°C, and the supernatant containing expressed Tm was decanted into a glass beaker. The supernatant was boiled for 6 min and allowed to cool for 45 min at room temperature. The denatured lysate containing Tm was purified from other bacterial proteins by three total cycles of acid/base cuts (or until a ratio of absorbance (A) at 260 nm and 280 nm [A_{260}/A_{280}] of <0.8 was reached): (1) precipitation of Tm by addition of 1 M HCl to pH ~4.5, (2) centrifugation at 28,950 $\times g$ for 10 min at 4°C, (3) resuspension of the pellets in 1 M KCl with addition of 1 M KOH to pH ~7, (4) centrifugation of the dissolved Tm at 28,950 $\times g$ for 10 min at 4°C, and (5) collection of the supernatant. Approximately 1 g of α -Tm dimer was purified from 2 liters of culture. Aliquots were stored at -80°C until use. For preparation of fluorescent Tm-actin, Tm (in 1 M KCl) was diluted 10-fold with M-ABB lacking KCl (bringing the final concentration of KCl to 0.1 M) and reconstituted overnight in a 3.5:1, 5:1, or 7:1 molar ratio of actin/Tm. In preliminary experiments, we tested cosedimentation of actin and Tm in 7:1 and 3.5:

1 mixtures. As expected for 7:1 actin/Tm, almost all of the Tm was bound to actin and observed in the F-actin pellet, and very low levels of Tm were in the supernatant. At the 3.5:1 actin/Tm ratio ~50% of the Tm pelleted with F-actin and 50% remained unbound in the supernatant (see supplemental Results and Discussion at bottom of the PDF).

Recombinant human cMyBP-C fragment preparations

pET45b vectors encoding *E. coli*-optimized codons for the C0-C1 or C0-C2 portion of human cMyBP-C with N-terminal 6x His tag and TEV protease cleavage site were obtained from GenScript. In addition, C0-C2 mutants were generated with HCM mutations (R282W, E334K, and L352P) or mutations in a positively charged loop (Arg-Ala-Ser-Lys [RASK]; residues 215-218) in the C1 domain that interacts with Tm (Risi et al., 2018). These Tm-binding mutations introduced additional positive charges (A216R/S217K) or reversed charges (R215E/K218E; Risi et al., 2018). Mutations were engineered in the human cMyBP-C fragments using a Q5 Site-Directed Mutagenesis Kit (New England Biolabs). All sequences were confirmed by DNA sequencing (Eton Biosciences). Protein production in *E. coli* BL21DE3-competent cells (New England Biolabs) and purification of C0-C1 and C0-C2 fusion proteins using His60 Ni Superflow resin were done as described previously (Bunch et al., 2018). C0-C2 and C0-C1 (with the His tag removed by TEV protease digestion) was then concentrated, dialyzed to 50/50 buffer (50 mM NaCl and 50 mM Tris, pH 7.5), and stored at 4°C. Initial characterization of conditions for TR-F was done with this protein, which was ~75% the correct molecular weight and 25% breakdown products (due to proteolysis within the motif between C1 and C2). For all of the TR-F binding curves and cosedimentation experiments, we further purified the C0-C2 using size exclusion chromatography to achieve >90% intact C0-C2. For size exclusion chromatography, C0-C2 (5-20 mg/ml, 1.7-2.5 ml) was applied in running buffer (150 mM NaCl, 50 mM NaPO₄, and 1 mM DTT, pH 6.7) to a HiPrep Sephacryl S-100 column. Flow rate was 0.7 ml/min. Purified C0-C2 was checked by SDS-PAGE for purity and then dialyzed into the appropriate buffer (usually M-ABB). The HCM mutant E334K was distinct from all other C0-C2 proteins in being highly destabilized in *E. coli* with many more breakdown products present during the purification process. These breakdown products were removed by size exclusion chromatography in the purification. We therefore measured only the effects of full-length E334K C0-C2. Proteins were typically used for experiments within 2 wk. For longer storage periods, C0-C2 and C0-C1 proteins were stored at -20°C in 50/50 buffer containing 50% glycerol, 1 mM DTT, protease inhibitors (88265, 1 tablet/50 ml; Pierce), and 1 mM sodium azide.

In vitro phosphorylation of cMyBP-C

For the determination of phosphorylated Ser residues, phosphorylation was monitored by in-gel staining of proteins with Pro-Q Diamond (Thermo Fisher Scientific) and staining total protein with SYPRO Ruby (Thermo Fisher Scientific), according to the supplier's instructions. Maximal phosphorylation was shown to plateau at ~2.5 ng PKA/ μg C0-C2 (Bunch et al., 2019). C0-C2 was typically treated with 7.5 ng PKA/ μg C0-C2 unless

otherwise noted. For liquid chromatography-tandem mass spectrometry (LC-MS/MS), CO-C2 WT and mutant R282W were treated with 65, 2.6, and 0.1 ng PKA/ μ g CO-C2. Phosphorylated proteins were separated by SDS-PAGE. The CO-C2 bands were excised as described previously (Bunch et al., 2018). Following LC-MS/MS, a probability-based approach for high-throughput protein phosphorylation analysis and site localization (Beausoleil et al., 2006) was used, as described previously for PKA treatment of WT CO-C2 (Bunch et al., 2019).

Actin cosedimentation assays

Actin binding by cMyBP-C fragments (CO-C2 or CO-C1) was determined by cosedimentation and analyzed as previously described in detail (Bunch et al., 2018). Binding levels were determined at 25°C in M-ABB using 1 μ M F-actin or 1 μ M F-actin containing 0.29 μ M Tm incubated with increasing amounts of CO-C2 or CO-C1. All cosedimentation curves were generated from at least two separate purifications of CO-C2 (and actin; $n > 4$ [typically $n = 6$] for all data points). All binding mixtures were made separately and not prepared in a single batch.

Determination of B_{\max} and K_d values

The maximum molar binding ratio (B_{\max}) and K_d values for CO-C2 binding to actin were determined by fitting the data to a quadratic model (Michaelis-Menten function) using Origin Pro 2019 computer software package through a nonlinear least-squares minimization (Levenberg-Marquardt algorithm). χ^2 values of quadratic fits for most binding experiments were < 0.005 . The exceptions to this are CO-C1, and the R215E/K218E mutant of CO-C2 when phosphorylated. In these cases, poor fits were due to much reduced, nonsaturable, binding and they instead fit to a linear function. These apparent K_d and B_{\max} values are used as comparative indicators of binding characteristics for CO-C2 binding to actin under different conditions (- and + phosphorylation or in the presence of mutations). They represent the apparent dissociation constants (CO-C2 concentration required for half-maximal binding) and maximal binding ratios of the cMyBP-C fragments to actin (CO-C2/actin) in cosedimentation experiments where bound cMyBP-C and total actin monomers are directly measured. In TR-F generated curves, the K_d values again represent the apparent dissociation constants (CO-C2 concentration required for half-maximal binding), but the B_{\max} in this case is the maximal change in lifetime of IAEDANS when CO-C2 binding is maximal. K_d values, expressed as μ M CO-C2 in both assays, can be compared within and between the two assays. The B_{\max} values, having different units in the two assays, can only be compared within the same type of assay (cosedimentation or TR-F). These values derived from fitting the data of the binding curves to a quadratic model (Michaelis-Menten function) are the standard values used to describe binding of cMyBP-C fragments to F-actin.

TR-F data acquisition

50 μ l of sample aliquots were loaded manually with a multi-channel pipette in 384-well black polypropylene microplates (#781209; Greiner Bio-One). Plates were spun for 1 min at 1,000 rpm (200 \times g) in an Eppendorf rotor (5810R A-4-81) to

remove air bubbles. Fluorescence lifetime measurements were acquired using a high-precision fluorescence lifetime plate reader (FLTPR; Fluorescence Innovations; Bunch et al., 2018; Schaaf et al., 2017). Dye-labeled F-actin (alone or mixed with CO-C2) was excited with either a 355-nm microchip laser (Teem Photonics) for IAEDANS, IAANS, and CPM dyes or a 473-nm microchip laser (Bright Solutions) for FMAL and IANBD dyes. Emission was filtered with 409-nm long-pass and 470/20-nm band-pass filters for the 355-nm laser (Bunch et al., 2018) or 488-nm long-pass and 517/20-nm band-pass filters (Semrock) for the 473-nm laser (Gruber et al., 2014). The FLTPR allows for high-throughput fluorescence lifetime detection at high precision by using unique direct waveform-recording technology (Muretta et al., 2010).

TR-F analysis

TR-F waveforms observed for each well were convolved with the instrument response function, and the lifetime (τ ; Eq. 1) was determined by fitting to a single-exponential decay using computer software (FLTPR, version 4.0.1; Fluorescence Innovations; and MATLAB, version 7.1; The MathWorks). The decay of the excited state of the fluorescent dye attached to actin at Cys-374 to the ground state is

$$I(t) = I_0 \exp(-t/\tau), \quad (1)$$

where I_0 is the fluorescence intensity upon peak excitation ($t = 0$) and τ is the fluorescence lifetime ($t = \tau$ when I decays to $1/e$ or $\sim 37\%$ of I_0).

High-throughput screening (HTS) data analysis

For suitability in HTS, TR-F assay quality was determined for various comparisons of sample conditions (i.e., unbound versus bound actin or unphosphorylated versus phosphorylated CO-C2). Typically, 40–60 wells of each condition were analyzed. To simulate future drug screens, 1% DMSO was added to each sample mixture. Sample mixtures were IAEDANS-actin, IAEDANS-actin + CO-C2, IAEDANS-actin + phosphorylated CO-C2, IAEDANS-actin-Tm, IAEDANS-actin-Tm + CO-C2, and IAEDANS-actin-Tm + phosphorylated CO-C2. Comparison of pairs of samples (sample A versus sample B) was indexed by the Z' factor, where a score of 0 to 0.5 indicates good and 0.5 to 1.0 indicates excellent assay quality (Zhang et al., 1999):

$$Z' = 1 - 3 \left(\frac{\sigma_A + \sigma_B}{\mu_A - \mu_B} \right), \quad (2)$$

where σ_A and σ_B are the SDs of the controls τ_A and τ_B , respectively, and μ_A and μ_B are the means of the controls τ_A and τ_B , respectively. Here, we make two sample A versus sample B comparisons: (1) unbound IAEDANS-actin (sample A) versus CO-C2-bound IAEDANS-actin (sample B) and (2) CO-C2 (-PKA treatment)-bound IAEDANS-actin (sample A) versus CO-C2 (+PKA treatment)-bound IAEDANS-actin (sample B). The same two comparisons were also done with IAEDANS-actin-Tm.

Statistics

Sample means are from four or more independent experiments. Each experiment, following the optimization of binding

conditions, was performed using at least two independent protein preparations. Average data are provided as mean \pm SE, except for Table 3 and Fig. 2, which used \pm SD for Z' scores. Statistical significance is evaluated by use of an unpaired *t* test. P values <0.05 were taken as indicating significant differences and are given in the figure and table legends as well as the Results section.

Online supplemental material

Actin TR-F-binding curves for mutants not included in the main text figures, comparison of the binding of specific substoichiometric levels of C0-C2 not included in the main text, comparisons of multiple or compounded variables (\pm PKA, Tm, mutation), and mass spectrometry details of phosphorylated C0-C2 proteins are included in the supplemental text. Testing of the four probes other than IAEDANS and further details of optimization of the experimental conditions for pH, salt, buffer, and Tm are also presented in the supplemental Results and Discussion sections. Specifically, Fig. S1 shows lifetime changes of five fluorescent dyes attached to actin at Cys-374 upon binding to C0-C2. Fig. S2 shows buffer conditions optimization of the TR-F assay for C0-C2 binding to IAEDANS-actin and IAEDANS-actin-Tm. Fig. S3 shows actin/Tm ratios. Fig. S4 shows TR-F IAEDANS-actin-Tm and IAEDANS-actin-binding curves for C0-C2 mutants. Fig. S5 shows effects of R282W HCM mutant on phosphorylation-modulated binding to actin-Tm at submaximal phosphorylation by PKA. Fig. S6 shows effects of Tm-binding mutants on phosphorylation-dependent binding to actin-Tm and actin. Fig. S7 shows cosedimentation assays for C0-C1 binding to actin-Tm and actin. Fig. S8 shows a comparison of TR-F and cosedimentation actin-binding assays for C0-C2 mutants. Table S1 lists TR-F and cosedimentation binding parameters of WT and mutant MyBP-C/actin and actin-Tm. Table S2 lists change in IAEDANS lifetime for IAEDANS-actin and IAEDANS-actin-Tm upon substoichiometric binding of C0-C2 and C0-C1. Table S3 lists WT and R282W C0-C2 phosphorylated peptides. Table S4 lists peak intensity ratios for WT and R282W PKA phosphorylated/unphosphorylated peptides.

Results

Actin-cMyBP-C TR-F biosensor

Our goal was to develop a TR-F-based actin-binding assay able to detect changes in actin binding of cMyBP-C brought about by different experimental conditions. A TR-F actin-binding assay in a 384-well plate format made possible the testing of variables such as pH, ionic strength, phosphorylation of cMyBP-C, and the presence of mutations in cMyBP-C. The results indicate that the assay will be useful in identifying therapeutic drugs that can modify cMyBP-C actin-binding properties to the same extent as phosphorylation. This same approach should be suitable, with appropriate modifications to the study of other ABPs.

Detailed optimization of probes, ionic strength and pH for the TR-F binding assay is presented in detail in the supplemental material. Using our current TR-F-binding assay, we monitored the lifetime of the thiol-reactive dye IAEDANS that is covalently attached to F-actin's readily labeled cysteine (Cys-374). The

buffer for actin-binding experiments was MOPS-Actin Binding Buffer (M-ABB; 100 mM KCl, 10 mM MOPS, pH 6.8, 2 mM MgCl₂, 0.2 mM CaCl₂, 0.2 mM ATP, 1 mM DTT, and 1 mM sodium azide). These conditions allowed us to readily distinguish between binding of C0-C2 that was unphosphorylated or phosphorylated (by PKA; Fig. 1 A) to actin or actin-Tm (Fig. 1 B). The addition of C0-C2 decreased the lifetime of IAEDANS-actin (with and without Tm) in a concentration-dependent manner. Upon phosphorylation of C0-C2 with PKA the decrease in IAEDANS-actin lifetime was much less, at submaximal binding concentrations of C0-C2 (Fig. 1 and Table 1). This indicates that PKA treatment reduced cMyBP-C binding to actin and actin-Tm (Fig. 1, A and B, dashed versus solid lines). These conditions also showed the presence of Tm on actin increases C0-C2 binding (Fig. 1 C, thick versus thin lines). At substoichiometric levels of binding (1.25 μ M C0-C2) Tm increased binding by 41% ($P < 0.005$; Table 2). We compared these data to results derived from cosedimentation experiments done under the same conditions (Fig. 1, D-F). Over the same concentration range, TR-F and cosedimentation assays provided similar binding profiles for unphosphorylated C0-C2, and these were linearly correlated (for actin and unphosphorylated C0-C2, $R^2 = 0.96$, adjusted- $R^2 = 0.95$; Fig. 1 G; and for actin-Tm, $R^2 = 0.87$, adjusted- $R^2 = 0.84$; Fig. 1 H). However, subtle differences in K_d and B_{max} are observed when fit to a quadratic equation for Michaelis-Menten binding kinetics (Table 1 or Fig. 1 G). Cosedimentation showed a less dramatic effect of PKA on binding actin compared with the TR-F assay (Fig. 1 D versus Fig. 1 A, and Table 1), while the effects were similar on actin-Tm (Fig. 1 E versus Fig. 1 B, and Table 1). The effect of PKA phosphorylation of C0-C2 is optimally seen when C0-C2 levels are below saturation (substoichiometric) at 2.5 μ M C0-C2 for actin (thin arrows in Fig. 1, A, C, D, and F) and 1.25 μ M C0-C2 for actin-Tm (thick arrows in Fig. 1, B, C, E, and F). This is the case for both TR-F and cosedimentation assays. For the TR-F assay, these concentrations showed the largest absolute difference in the change in lifetime between minus and plus PKA of 1.7% and 2.0% (Table 2). These equate to PKA treatment of C0-C2 reducing the change in lifetime of IAEDANS on actin by 66% and 74% compared with the change in lifetime observed when C0-C2 was not phosphorylated (Table 2). These concentrations (2.5 μ M C0-C2 for actin and 1.25 μ M C0-C2 for actin-Tm) also result in the highest levels of statistical significance when comparing \pm PKA ($P = 2.9 \times 10^{-11}$ for actin and $P = 1.6 \times 10^{-13}$ for actin-Tm).

Z' score evaluation of TR-F binding assays for HTS

We used Z' scores to determine if our actin-cMyBP-C TR-F assay has sufficient sensitivity for employment in HTS. We are interested in screening chemical libraries to identify drugs that affect binding of cMyBP-C or that mimic the effects of phosphorylation of cMyBP-C on actin binding. Z' scores (see Eq. 2 in Materials and methods) allow for the determination of whether the signal window ($\Delta\tau$) between two states (bound versus not bound, or phosphorylated binding versus not phosphorylated binding) and the variance (SD) of the two states indicate a worthless HTS (Z' score <0), a doable HTS (Z' score 0–0.5) or an excellent HTS assay quality (Z' score 0.5–1.0; see also Fig. 2, D

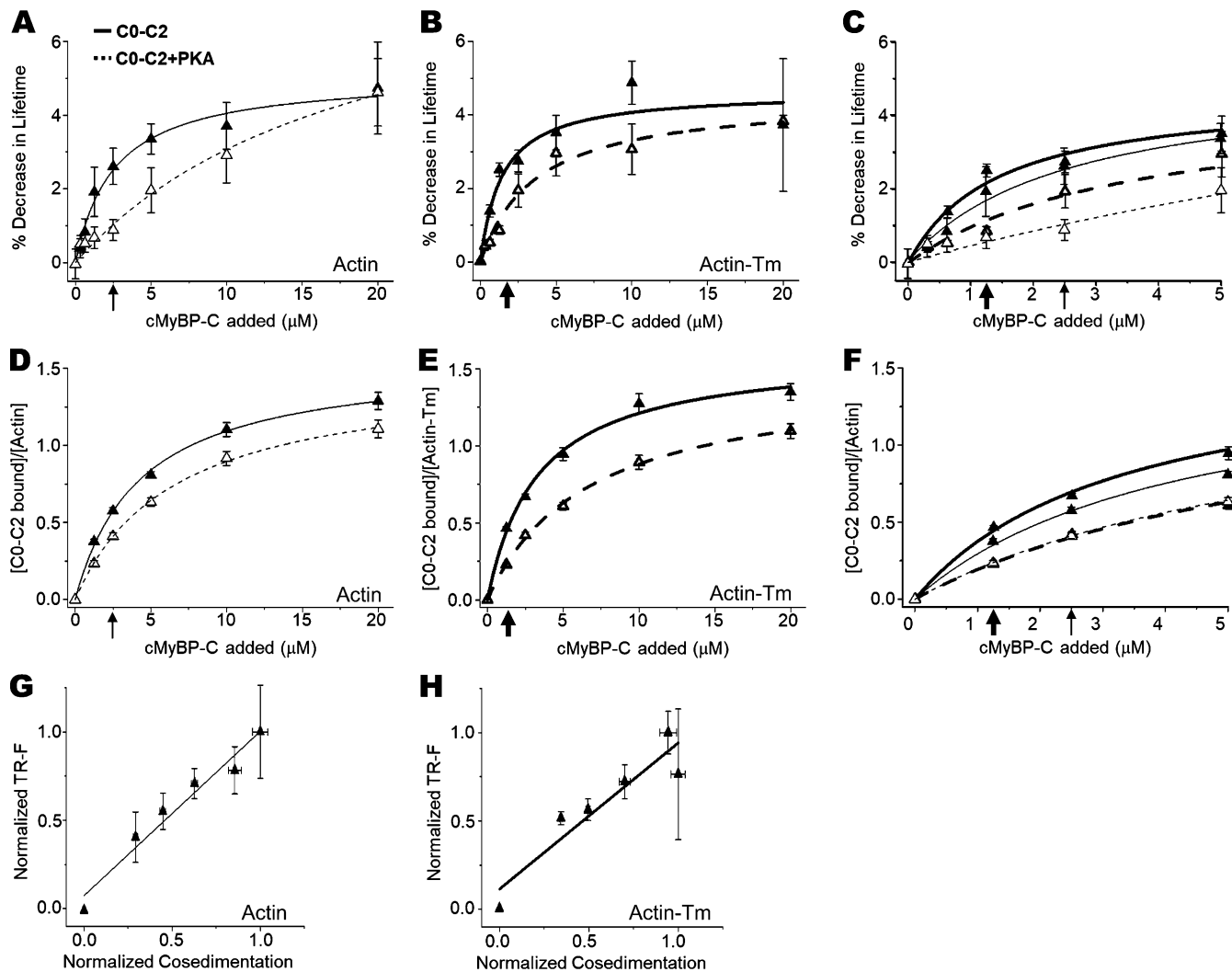


Figure 1. TR-F binding assays for actin and actin-Tm compared with cosedimentation. Unphosphorylated C0-C2 (solid lines) and phosphorylated C0-C2 (dotted lines) were assayed. **(A)** TR-F using IAEDANS-actin (thin lines). **(B)** TR-F using IAEDANS-actin-Tm (thick lines). **(C)** TR-F using IAEDANS-actin and IAEDANS-actin-Tm showing 0–5 μM C0-C2 added. **(D)** Cosedimentation using actin. **(E)** Cosedimentation using actin-Tm. **(F)** Cosedimentation using IAEDANS-actin and IAEDANS-actin-Tm showing 0–5 μM C0-C2 added. Arrows in A–F indicate the C0-C2 concentrations to be used in future screens (thin arrows, 2.5 μM for actin alone; thick arrows, 1.25 μM for actin-Tm). **(G)** Linear correlation plot of unphosphorylated C0-C2 binding measured by TR-F (change in lifetime) and cosedimentation ($[\text{bound C0-C2}]/[\text{actin}]$) for actin ($R^2 = 0.96$) with each assay readout normalized to 1 (at 20 μM C0-C2). **(H)** Linear correlation plot in the presence of Tm, under conditions of G_1 , for unphosphorylated C0-C2 binding to actin-Tm ($R^2 = 0.87$). Refer to [Table 1](#) for statistical analysis of fitted binding properties for curves. Data are provided as mean \pm SE ($n > 4$).

and E). Using either the IAEDANS-actin or IAEDANS-actin-Tm sensor, we performed a simulated HTS by loading ~ 60 wells of each condition in 384-well plates. The conditions tested were: actin alone, actin plus C0-C2, and actin plus PKA-treated C0-C2 as well as actin-Tm alone, actin-Tm plus C0-C2, and actin-Tm plus PKA-treated C0-C2. Means and three SDs ($3 \times \text{SDs}$) of the lifetimes for each condition were used to determine the Z' scores (see [Fig. 2](#)). The Z' score for the screen shown in [Fig. 2](#) was calculated as $Z' = 0.56$ for IAEDANS-actin alone versus IAEDANS-actin plus C0-C2 and $Z' = 0.27$ for IAEDANS-actin plus C0-C2 versus IAEDANS-actin plus PKA-treated C0-C2. The Z' score determination was performed in triplicate with three different IAEDANS-actin (and IAEDANS-actin-Tm) and C0-C2 preparations. All tests gave Z' scores that indicated good (doable) or excellent screening quality. Actin-Tm showed higher scores

(average $Z' = 0.46$) than actin alone (average $Z' = 0.29$; [Table 3](#)). These results validate the robustness of TR-F for HTS.

Effects of cMyBP-C HCM and Tm-binding mutations on actin binding detected by TR-F

The ability of the TR-F binding assay to quickly and reproducibly distinguish between two states of cMyBP-C suggests that it will be useful in probing the effects of mutations in cMyBP-C (and potentially other ABPs) on actin binding. Importantly, the ability to detect effects of mutations on actin binding would serve as a proof of principle that the assay can detect other factors, such as therapeutic drugs, that modulate binding. For these reasons, we tested the sensitivity of the TR-F assay to detect changes in C0-C2 binding due to three HCM mutations predicted from previous work to affect actin binding in very different manners.

Table 1. TR-F and cosedimentation binding parameters of cMyBP-C C0–C2 binding to actin and actin–Tm

Filament	PKA	TR-F		Cosedimentation	
		K_d (μM)	B_{max} (maximal $\Delta\tau$)	K_d (μM)	B_{max} (fraction bound; C0–C2/actin)
Actin	–	2.5 \pm 0.4	5.1 \pm 0.3	4.3 \pm 0.3	1.56 \pm 0.04
Actin	+	19 \pm 5 ^a	9 \pm 1 ^a	6.5 \pm 0.3 ^a	1.48 \pm 0.03
Actin–Tm	–	1.4 \pm 0.5 ^b	4.6 \pm 0.4	3.3 \pm 0.4	1.61 \pm 0.06
Actin–Tm	+	3.6 \pm 0.7 ^{a,c}	4.5 \pm 0.3 ^c	6.6 \pm 0.4 ^a	1.46 \pm 0.04

Data are mean \pm SE ($n > 4$) for a binding curve of eight concentrations of C0–C2 (0–20 μM) to 1 μM of actin (Fig. 1) fit to a quadratic equation. Significant difference due to PKA treatment (– versus + PKA rows).

^a $P < 0.05$. Significant difference due to presence of Tm (actin versus actin–Tm rows of same PKA condition).

^b $P = 0.10$. Units for B_{max} are lifetime change (maximal $\Delta\tau$) for TR-F and fraction of actin bound (C0–C2/actin) for cosedimentation.

^c $P < 0.05$. Trending difference in K_d due to presence of Tm. See Discussion for a detailed discussion of K_d and B_{max} uses and limitations.

Previous work suggested L352P increases actin binding and E334K decreases binding. We predicted that R282W, based on sequence analysis, alters phosphorylation and would thereby alter actin binding. We also tested two mutations in a proposed Tm-binding sequence in C1. The location of these mutations is diagrammed in Fig. 3. The key comparisons that validate the assay's usefulness to detect a variety of changes in binding due to mutations are presented in Figs. 4, 5, and 6 and Table 2. As the assay makes possible the comparison of combinations of

Table 2. Change in IAEDANS lifetime for IAEDANS–actin and IAEDANS–actin–Tm upon substoichiometric binding of C0–C2 and C0–C1

cMyBP-C complex with 1 μM F-actin	IAEDANS	Change in IAEDANS lifetime (%)	
		–PKA	+PKA
C0–C2 WT (2.5 μM)	Actin	2.61 \pm 0.14	0.88 \pm 0.08
C0–C2 WT (1.25 μM)	Actin	1.92 \pm 0.17	0.68 \pm 0.08
C0–C2 WT (0.625 μM)	Actin	0.83 \pm 0.1	
C0–C2 WT (1.25 μM)	Actin–Tm	2.70 \pm 0.07	0.71 \pm 0.06
C0–C2 WT (0.65 μM)	Actin–Tm	1.70 \pm 0.12	
C0–C2 WT (0.0313 μM)	Actin–Tm	0.56 \pm 0.06	
C0–C1 ($\Delta\text{m-C2}$; 2.5 μM)	Actin	0.17 \pm 0.06	
C0–C2 L352P (2.5 μM)	Actin	3.62 \pm 0.19	
C0–C2 E334K (2.5 μM)	Actin	2.79 \pm 0.11	
C0–C2 R282W (2.5 μM)	Actin	2.20 \pm 0.24	0.86 \pm 0.12
C0–C2 R282W (1.25 μM)	Actin	1.24 \pm 0.12	0.53 \pm 0.08
C0–C2 R215E/K218E (1.25 μM)	Actin	0.77 \pm 0.06	
C0–C2 R215E/K218E (1.25 μM)	Actin–Tm	0.48 \pm 0.05	
C0–C2 A216R/S217K (1.25 μM)	Actin	2.63 \pm 0.10	
C0–C2 A216R/S217K (0.625 μM)	Actin	2.16 \pm 0.13	
C0–C2 A216R/S217K (1.25 μM)	Actin–Tm	2.98 \pm 0.08	
C0–C2 A216R/S217K (0.625 μM)	Actin–Tm	2.68 \pm 0.05	
C0–C2 A216R/S217K (0.313 μM)	Actin–Tm	2.08 \pm 0.12	

Substoichiometric binding levels of cMyBP-C C0–C2 and C0–C1 on 1 μM IAEDANS-labeled actin and actin–Tm. Data are provided as mean \pm SE ($n > 4$). P values comparing different samples are given in Results.

multiple factors (minus and plus HCM or Tm-binding mutations, minus and plus phosphorylation by PKA, minus and plus Tm) this was done as well and is presented in the supplemental material.

C0–C1 decreases actin binding

The M-domain and C2 provide binding sites for actin (Howarth et al., 2012; Bezold et al., 2013) and their removal, in C0–C1, dramatically reduces actin binding and this is seen in the TR-F assay as well (Fig. 4 and Table 2; >90% reduction in binding at 2.5 μM , $P < 0.0001$).

L352P increases actin binding

The L352P mutation has been demonstrated to increase actin (Bezold et al., 2013) and thin filament (Mun et al., 2016) binding. The TR-F assay readily detected the increase in binding of L352P to actin (Fig. 4 and Table 2). Increases of 39% were seen at 2.5 μM L352P C0–C2 ($P < 0.0005$).

E334K does not alter actin binding

The HCM mutant, E334K, was tested because it significantly reduced actin binding when present in mouse C1–C2 (Bezold et al., 2013) and the homologous mutant (E330K) in mouse hearts shortened the duration of ejection (van Dijk et al., 2018). E334K in human C0–C2 displayed binding that was similar to WT measured by TR-F (Fig. 4 and Table 2).

R282W alters phosphorylation and actin binding

R282W changes the PKA target sequence (281–284) from RRIS to RWIS (Fig. 3), and this change is predicted to eliminate PKA phosphorylation of Ser-284. Ser-284 is one of four serines in the M-domain phosphorylated by PKA (Jia et al., 2010; Ponnamm et al., 2019; O'Leary et al., 2019). We predicted that R282W would eliminate PKA phosphorylation of this serine. Under our standard conditions, R282W showed subtle, but not significant, differences in binding when compared with WT in either the phosphorylated or unphosphorylated state at 2.5 μM . At 1.25 μM , unphosphorylated R282W did display a significant decrease in binding (36% decrease, $P < 0.01$; Fig. 5 and Table 2).

Examination by mass spectrometry of the four serines (Ser-275, Ser-284, Ser-304, and Ser-311) in the motif that are

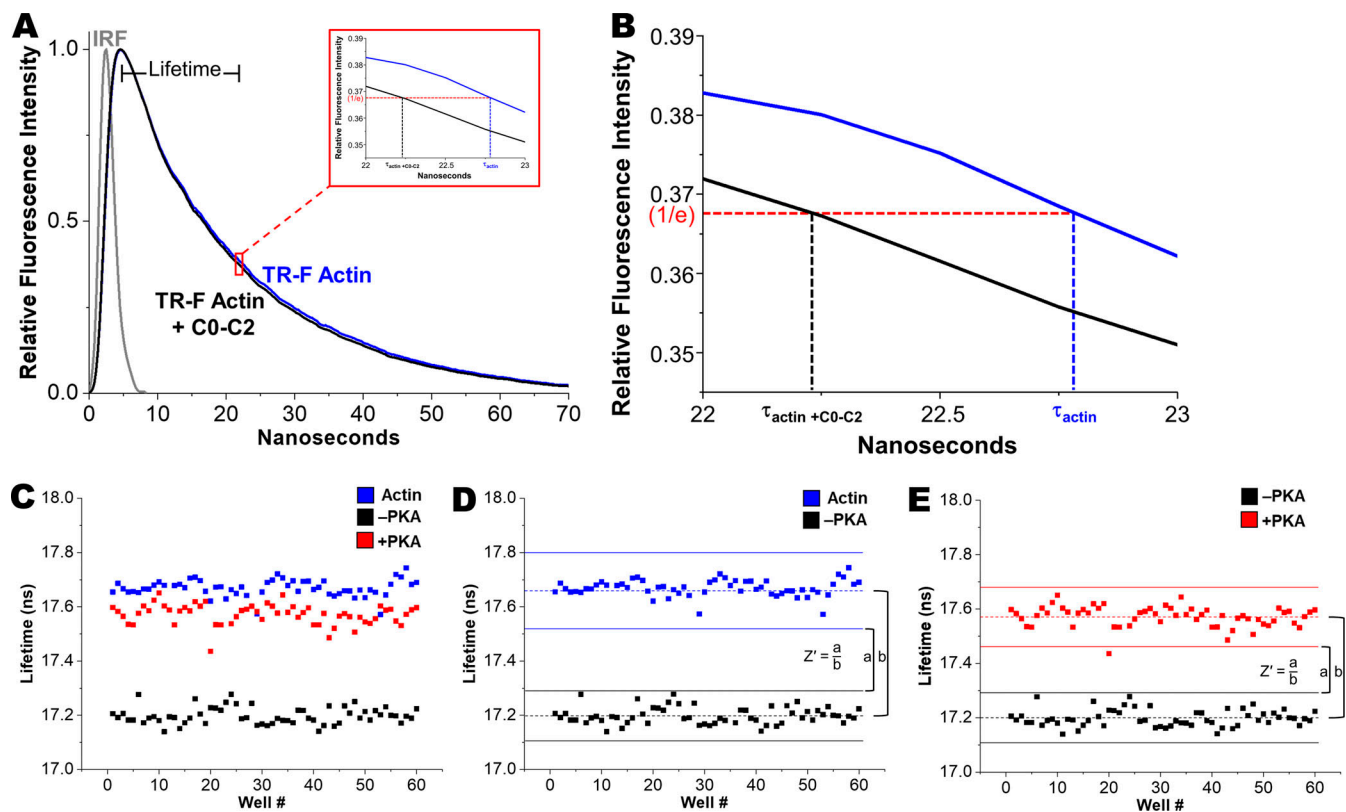


Figure 2. Example of Z' score calculation for TR-F of IAEDANS-labeled F-actin binding to unphosphorylated and phosphorylated C0-C2. (A) Fluorescence waveform of IAEDANS-labeled F-actin (blue line) and the same together with 20 μ M C0-C2 (black line; both normalized to their maximum intensity values) and the instrument response function (IRF; gray line). Red box (inset) highlights Relative Fluorescence Intensity $\sim 1/e$ magnified to show difference in TR-F lifetimes of actin and actin + C0-C2. This is expanded further in B. (B) Magnified view of lifetime differences from red box in A. The actual lifetimes (~ 17.5 ns, shown in C-E) are the times shown on the x axis to reach $1/e$ of the peak intensity (~ 22.5 ns) minus the time to reach peak intensity (~ 5 ns in the convoluted fluorescence waveform; see peak in A). (C) Lifetimes measured in a 384-well plate containing 60 wells each of 1 μ M IAEDANS-actin alone (blue), actin plus 2.5 μ M C0-C2 (black), or actin plus 2.5 μ M PKA-treated C0-C2 (red). (D) Comparing actin alone to actin plus C0-C2. (E) Comparing actin plus C0-C2 versus actin plus PKA-treated C0-C2. For D and E, horizontal solid lines indicate $3 \times$ SD of the mean lifetime (dotted line). Z' score is defined as the difference between $3 \times$ SD (a) divided by the difference in the mean signal (b) in D and E. While comparisons made in D and E, having no overlap at $3 \times$ SD, are clearly significantly different, note that even the difference between actin alone and actin bound to phosphorylated C0-C2 (blue versus red in C) is also significant ($P < 0.0001$).

phosphorylated by PKA showed that at PKA levels required for maximal phosphorylation (2.5 ng PKA/ μ g C0-C2) or 25 times those levels, all four serines were phosphorylated in WT C0-C2. In contrast, in the R282W mutant, phosphorylation was almost undetectable at Ser284. Phosphorylation was detected in the mutant at Ser-275, Ser-304, and Ser-311 (Table S3 and Table S4). The initial test of PKA effects on actin binding used PKA levels three times that required for maximal phosphorylation. From these results, we concluded that phosphorylation in some combination of Ser-275, Ser-304, and Ser-311 in R282W is sufficient to reduce interactions with actin.

In vivo, the PKA target serines are not found completely phosphorylated (Copeland et al., 2010; Jacques et al., 2008). We therefore tested a range of phosphorylation levels of C0-C2 for their effects on binding to actin. As for testing other conditions, use of the TR-F assay in a 384-well plate format made this relatively easy. We reduced the PKA levels used to phosphorylate WT and R282W C0-C2 for actin-binding studies. The effect of submaximal phosphorylation on the change in TR-F upon binding to actin was measured. Immediately following

determination of the TR-F, a portion of the samples was removed with a multichannel pipette and placed in protein sample buffer, run on SDS-PAGE gels, and stained with Pro-Q Diamond to determine phosphorylation levels. A wide range of phosphorylation levels was obtained by varying PKA levels, and the R282W mutant was less phosphorylated than WT at all PKA concentrations (Fig. 5, B and C). At levels of phosphorylation mediated by PKA at 1.5 ng PKA/ μ g C0-C2, binding of WT C0-C2 remained low, at the same level as that seen when either it or R282W was treated with 5 ng PKA/ μ g C0-C2. R282W, at this concentration (1.5 ng PKA/ μ g C0-C2), showed a 65% increase in binding to actin (Fig. 5 D; $P < 0.00001$). As PKA levels were reduced further to 0.5 ng PKA/ μ g C0-C2, the difference between WT and the mutant remained significant (Fig. 5 D; 27%, $P = 0.0009$), though both now exhibited increased binding.

Mutations in the RASK sequence in C1 affect actin-Tm binding
Binding to actin by C0-C2 is increased when actin is decorated with Tm (Fig. 1, C and F; and Table 1). To specifically investigate the ability of the TR-F screen to detect changes in cMyBP-C

Table 3. **Z' score quality calculation for potential actin C0–C2 binding screens**

(#) Preparation	PKA	n	Lifetime (ns)	3× SD (ns)	Z' score
(1) Actin alone	-	48	17.53	0.08	
(1)					Actin ± C0–C2 0.43
(1) Actin + C0–C2	-	58	16.97	0.24	
(1)					Actin C0–C2 ± PKA 0.07
(1) Actin + C0–C2	+	60	17.34	0.10	
(2) Actin alone	-	57	17.68	0.08	
(2)					Actin ± C0–C2 0.56
(2) Actin + C0–C2	-	60	17.22	0.13	
(2)					Actin C0–C2 ± PKA 0.27
(2) Actin + C0–C2	+	59	17.54	0.11	
(3) Actin alone	-	10	17.59	0.25	
(3)					Actin ± C0–C2 0.12
(3) Actin + C0–C2	-	49	17.06	0.21	
(3)					Actin C0–C2 ± PKA 0.26
(3) Actin + C0–C2	+	48	17.49	0.10	
(1) Actin–Tm alone	-	60	17.52	0.08	
(1)					Actin–Tm ± C0–C2 0.51
(1) Actin–Tm + C0–C2	-	60	16.91	0.21	
(1)					Actin–Tm C0–C2 ± PKA 0.26
(1) Actin–Tm + C0–C2	+	58	17.39	0.09	
(2) Actin–Tm alone	-	48	17.66	0.14	
(2)					Actin–Tm ± C0–C2 0.50
(2) Actin–Tm + C0–C2	-	58	17.20	0.09	
(2)					Actin–Tm C0–C2 ± PKA 0.45
(2) Actin–Tm + C0–C2	+	60	17.57	0.11	
(3) Actin–Tm alone	-	10	17.60	0.08	
(3)					Actin–Tm ± C0–C2 0.57
(3) Actin–Tm + C0–C2	-	48	17.09	0.14	
(3)					Actin–Tm C0–C2 ± PKA 0.45
(3) Actin–Tm + C0–C2	+	49	17.51	0.09	

Three separate preparations of actin and C0–C2 were used (1, 2, and 3) to run mock plate reader screens for calculating Z' score using Eq. 2 (see Materials and methods) based on mean lifetime (nanoseconds) and SD. For binding experiments using IAEDANS–actin, 2.5 μM C0–C2 was added. 1.25 μM C0–C2 was used for IAEDANS–actin–Tm. Binding was done with (+) or without (–) PKA treatment to phosphorylate cMyBP-C. Within each preparation, actin alone was compared to actin with bound C0–C2 for one comparison (actin ± C0–C2; first row versus second row for each preparation). Actin bound to unphosphorylated versus phosphorylated C0–C2 was also compared (actin C0–C2 ± PKA; second row versus third row for each preparation). See Fig. 2, C–E, for a representative example of the mock screen.

interactions with Tm, we made functional mutations in the C1 domain in a region (amino acids 215–218; RASK) that interacts with Tm (Risi et al., 2018). Mutating this sequence to EASE (R215E/K218E; changing the positively charged R and K to the negatively charged E) resulted in 82% lower levels of binding to actin–Tm at 1.25 μM when compared with WT ($P < 1 \times 10^{-13}$). This mutant, EASE, displayed 37% lower levels of binding at 1.25 μM C0–C2 to actin–Tm than to actin alone ($P = 0.026$; Fig. 6, A and B; and Table 2). This is the only mutation tested that resulted in less binding to actin–Tm than to actin. In contrast, WT C0–C2 shows a 41% greater TR–F effect on actin–Tm than on actin alone ($P = 0.003$; Fig. 1 and repeated in Fig. 6 and Table 2). Addition of positively charged amino acids to the Tm-binding region, RRKK (A216R/S217K), enhanced binding at 1.25 μM C0–C2 compared with WT to actin–Tm by 10% ($P = 0.021$). At lower concentrations of 0.625 and 0.313 μM, these relative differences were even greater (58% and 275%, respectively; $P < 1 \times 10^{-6}$; Fig. 6 D and Table 2). The results with Tm-binding region mutants are

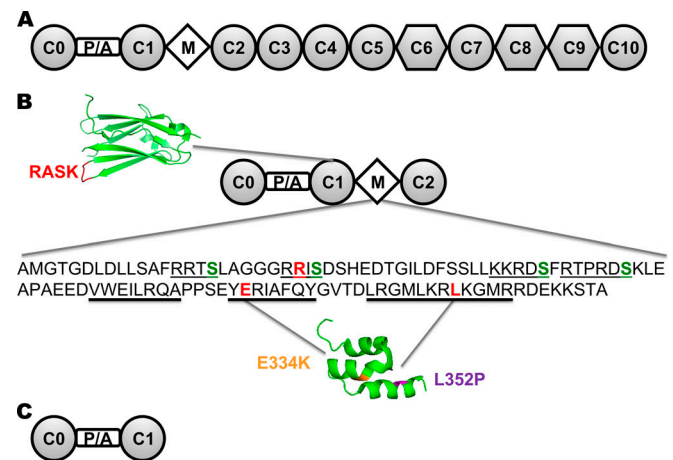


Figure 3. **cMyBP-C organization and C0–C2 mutants tested.** (A) Full-length cMyBP-C domains C0–C10. Ig-like domains shown as circles and Fn3-like domains as hexagons. (B) C0–C2 domains containing P/A linker and phosphorylatable M-domain are shown. Sequence of M-domain and locations of HCM mutations tested for binding. PKA phosphorylatable Ser residues are in green, PKA recognition sequences are indicated with underlines, and HCM mutation sites are in red. Helix residues in the tri-helix bundle are indicated with thick underlines. Structure insets: tri-helix bundle (Michie et al., 2016; PDB accession no. 5K6P) containing L352P and E334K mutations and C1 (Risi et al., 2018; PDB accession no. 6CXI) showing the RASK loop between adjacent β-strands that interacts with Tm. (C) C0–C1 is a deletion of the M-domain and C2.

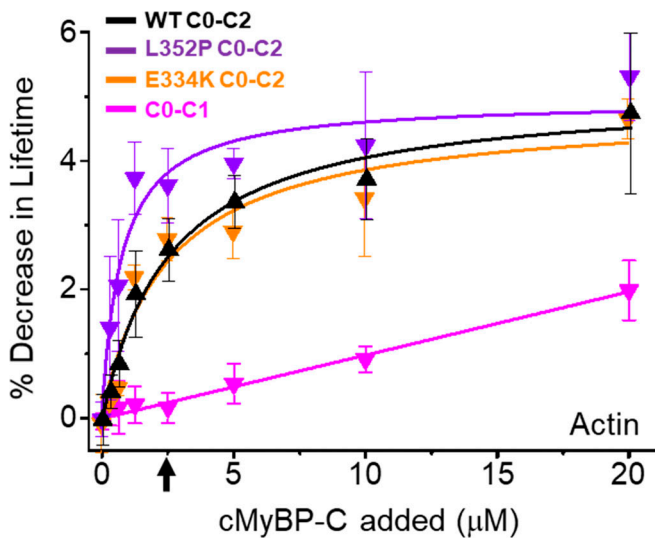


Figure 4. **TR-F binding curves of WT C0-C2, L352P, E334K, and C0-C1 on IAEDANS-actin.** TR-F of IAEDANS-actin binding to 0–20 μM C0-C2 and C0-C1. Data are provided as mean \pm SE ($n > 4$).

consistent with effects of the same mutants tested in C0-C1 for effects on thin filament activation of myosin ATPase (Risi et al., 2018). On actin alone, at lower concentrations (1.25 and 0.625 μM C0-C2), the RRKK increased binding by 37% and 160% compared with WT ($P < 0.006$; Fig. 6 D and Table 2). The

negative (EASE) mutation had negative effects on binding to bare actin as well. Binding was reduced by 60% ($P < 0.001$) at 1.25 μM C0-C2 when compared with WT on actin, but these effects were reduced compared with those with actin-Tm (Fig. 6 B and Table 2).

Discussion

We found that TR-F can be used to monitor the binding of the N-terminal domain of cMyBP-C (C0-C2) to actin and actin-Tm. The 384-well plate format allowed us to quickly and easily optimize conditions for TR-F monitoring of binding. We optimized the conditions to detect both differences between the binding of phosphorylated and unphosphorylated C0-C2 and increased binding provided by the presence of Tm on the actin filament. Using these conditions, we characterized the assay's ability to detect differences in binding due to phosphorylation, Tm, or mutations in C0-C2. These tests all indicate that this assay will be suitable for screening drug libraries to identify molecules capable of modulating cMyBP-C's ability to bind actin and actin-Tm, potentially through mimicking phosphorylation of the M-domain. Z' score analysis adds additional confidence to the appropriateness of this new method for HTS.

TR-F changes due to C0-C2 binding to actin are highly significant and not probe dependent

All five fluorescent probes we tested reported a reduction in lifetime upon binding (Fig. S1). The finding that all the

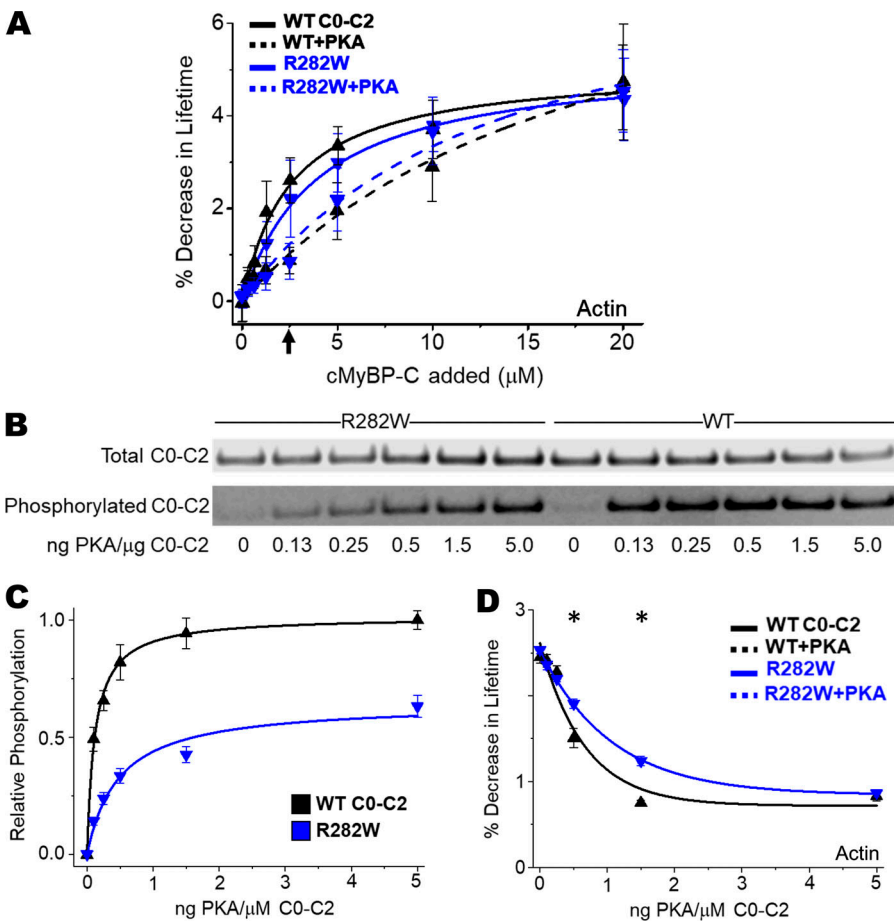


Figure 5. **Effects of WT and R282W HCM mutant on phosphorylation-modulated binding to actin at submaximal phosphorylation by PKA.** (A) TR-F of IAEDANS-actin incubated with increasing concentrations of C0-C2 (WT, black; R282W, blue) either unphosphorylated (solid lines) or phosphorylated using 7.5 ng PKA/ μg C0-C2 (dashed lines). For B–D, effects of HCM mutant R282W on C0-C2 phosphorylation were tested over a range of PKA levels (0–5 ng PKA/ μg C0-C2). (B) SYPRO Ruby (total protein; top bands) and Pro-Q Diamond (phosphorylated protein; bottom bands) stains of SDS-PAGE. (C) Relative phosphorylation levels of WT and R282W (normalized to the ratio of the Pro-Q Diamond/SYPRO Ruby intensities for WT C0-C2 at 5 ng PKA/ μg C0-C2). Phosphorylation levels of R282W are significantly different ($P < 0.00006$) from WT for all concentrations of PKA. (D) WT and R282W effects on IAEDANS-actin lifetime change as a function of PKA concentration. At intermediate phosphorylation levels (0.5 and 1.5 ng PKA/ μM C0-C2), binding to actin detected by TR-F is significantly different between WT and R282W (*, $P < 0.003$). Average data are provided as mean \pm SE ($n > 4$).

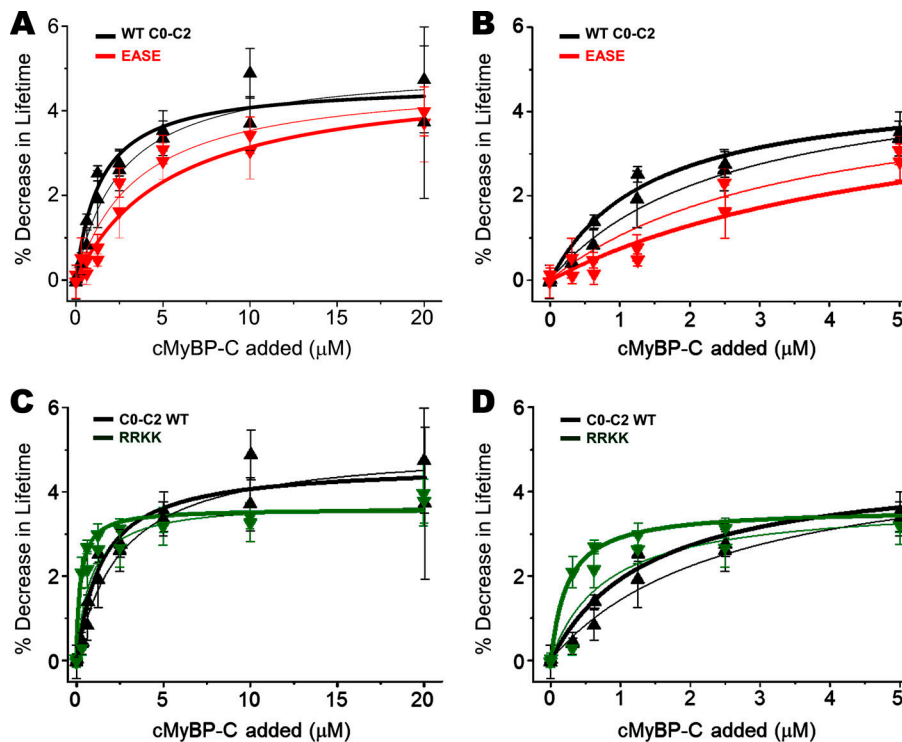


Figure 6. Effects of WT and Tm-binding mutants on binding to actin-Tm and actin. Effects of WT and Tm-binding mutants on actin-Tm (thick lines) and actin (thin lines) TR-F were tested. Tm-binding mutants reverse charges (EASE; R215E/K218E) or introduce additional positive charges (RRKK; A216R/S217K) in the Tm-binding loop 215–218, RASK, of C0–C2. **(A)** WT and R215E/K218E (EASE in red) effects on IAEDANS-actin-Tm and IAEDANS-actin for C0–C2 from 0 to 20 μM . **(B)** Zooming in on the lower concentrations (0–5 μM) C0–C2 added in A. **(C and D)** The same conditions as A and B above but comparing WT and A216R/S217K (RRKK in green). For the Tm-binding mutant (charge reversal-EASE), apparent K_d changes trended toward significant ($P = 0.11$) for actin-Tm, but not for actin alone. For the positive Tm-binding mutant (additional positive charges-RRKK), apparent K_d changes were significant ($P < 0.05$) for binding to both actin and actin-Tm. Refer to Table S1 for statistical analysis of fitted binding properties for curves and Table 2 for comparisons of binding at specific C0–C2 concentrations. Data are provided as mean \pm SE ($n > 4$).

fluorescent probes showed reduced lifetimes indicates that the results we are seeing are due to C0–C2 interactions with actin and not with a specific probe attached to actin’s Cys-374. Cryo-electron microscopy of thin filaments decorated with C0–C1 (Risi et al., 2018) found C1 binds predominantly in what they termed the C1-S structural class. This class of binding is characterized by, among other contacts, residues 194–206 of C1 interacting with residues 365–367 of actin (Harris et al., 2016). Actin’s Cys-374 is labeled by our probes. This site is in close proximity to this C1-actin interaction region. Though we do not yet have a structure for C0–C2 binding to thin filaments, this C1-actin interaction in close proximity to Cys-374, may explain the responsiveness of all the probes to C0–C2 binding. We selected IAEDANS-actin for optimization as it displayed the largest change in lifetime upon binding C0–C2 and had low variability. IAEDANS-actin readily distinguished between the binding observed with C0–C2 in its phosphorylated versus unphosphorylated state.

Lifetimes for IAEDANS attached to actin ranged from 16.5 to 18 ns with 0.3- to 1.1-ns changes upon binding to C0–C2. These lifetime changes appear small ($\sim 2.7\%$), but on a biophysical scale they are very significant, with SEs on the order of ~ 5 –50 ps (or 0.01–0.05%).

Wide-ranging flexibility and easy optimization of fluorescence lifetime-based binding assay

The TR-F assay in the 384-well format makes testing a wide range of conditions relatively easy. Numerous variables can be rapidly tested for scientific discovery and optimization of assay conditions. Our testing of conditions for optimal binding (see Fig. S2) suggested that the assay can be used in wide range of ionic strength and pH conditions. Subtle differences were

observed. Lower pH (6.8) showed larger differences between binding of unphosphorylated and phosphorylated C0–C2 compared with that seen at pH 7.5 or pH 8.0 (Fig. S2 A). The higher pH conditions displayed larger differences between actin and actin-Tm binding. Replacing the KCl in our standard buffer with NaCl increased the difference between unphosphorylated and phosphorylated binding but reduced the effects of Tm. Having the ability to test all of these conditions (Fig. S2, A–C; and Fig. S3) allowed us to select buffer conditions that balanced phosphorylation and Tm effects. We would not have attempted this optimization using standard cosedimentation assays. The buffer we opted for is M-ABB (100 mM KCl, 10 mM MOPS, pH 6.8, 2 mM MgCl_2 , 0.2 mM CaCl_2 , 0.2 mM ATP, 1 mM DTT, and 1 mM sodium azide).

Using the TR-F-optimized conditions, we retested binding by cosedimentation assays. The new conditions led to an increase in binding affinity, as measured by cosedimentation over our previous conditions (Bunch et al., 2019). Previously, using 1 μM phalloidin-stabilized F-actin in cosedimentation assays, we observed apparent K_d values for C0–C2 binding to actin of $11 \pm 2 \mu\text{M}$ (unphosphorylated) and $10 \pm 4 \mu\text{M}$ (phosphorylated). Using our new conditions, we find apparent K_d values, measured by cosedimentation, to be $4.3 \pm 0.3 \mu\text{M}$ (unphosphorylated) and $6.5 \pm 0.3 \mu\text{M}$ (phosphorylated). The K_d values also indicate that in addition to decreased K_d values (increased affinities), we now observe larger differences in binding, measured by cosedimentation, between unphosphorylated and phosphorylated C0–C2 (Table 1 and Fig. 1 D). We conclude that the TR-F assay, in the 384-well plate format, can be used to probe physiological and chemical variables of actin binding, and these findings can be transferable to different complementary assays.

Use of substoichiometric levels of C0–C2 for comparison of binding by C0–C2 variants

While K_d and B_{max} values are useful for comparing binding curves, it is questionable how relevant the numbers are to in vivo binding. Binding is likely to be complex under the conditions required to generate in vitro binding curves, as each actin monomer in the F-actin possesses multiple interaction sites for C0–C2. Likewise, C0–C2 possesses multiple binding sites for multiple actin regions (Shaffer et al., 2009; Orlova et al., 2011; Risi et al., 2018). At elevated C0–C2 concentrations, competition between sites, cooperative interactions, and steric hindrance are all likely to be significant. In vivo, high ratios of C0–C2/actin (greater than 1:7) are not present, and therefore, neither competition nor steric hindrance is a factor. Due to these complexities, we show the binding curves (Figs. 1, 4, 5, 6, S4, S5, S6 and S7) as well as report apparent K_d and B_{max} values (Tables 1 and Table S1). Visual inspection of each curve confirms that when lower K_d values are observed, more binding is observed at low (substoichiometric) C0–C2/actin levels that are more physiologically relevant (in muscle, cMyBP-C is present at approximately one out of every seven actin monomers). For this reason, we have extracted, from the curves, the binding levels observed at substoichiometric concentrations of C0–C2 for direct comparison in Tables 2 and Table S2.

Tm enhanced cMyBP-C binding to IAEDANS–actin: impacts on mechanistic and therapeutic discovery

After establishing that IAEDANS labeling of actin at Cys-374 is suitable as a biosensor to detect cMyBP-C binding, we aimed to increase the physiological relevance of the bound complex by including cardiac Tm in the assay. For studies of cardiac and skeletal muscle actin, Tm is a key regulatory protein of contraction that blocks the myosin-binding sites on actin. cMyBP-C has been proposed to interact with Tm. These interactions directly modulate Tm's position on actin independent of Ca^{2+} activation in cardiac thin filaments (Risi et al., 2018). The TR-F assay worked well using IAEDANS–actin–Tm to detect cMyBP-C binding. The presence of Tm enhanced binding at low C0–C2 concentrations. This suggests that Tm facilitates binding, consistent with cMyBP-C's proposed interactions with both F-actin (Orlova et al., 2011; Harris et al., 2016) and Tm (Mun et al., 2014; Risi et al., 2018). We conclude that the TR-F assay is suited for detecting binding with either actin or actin–Tm.

These findings set the stage for screening for drugs that modulate cMyBP-C (in either the phosphorylated or unphosphorylated state) binding to actin–Tm. Screening using IAEDANS–actin–Tm offers potential benefits over using IAEDANS–actin. First, due to increased binding detected by TR-F, the presence of Tm reduces the concentration of C0–C2 required to observe the greatest difference between the phosphorylated and unphosphorylated forms (down to 1.25 μ M C0–C2 from the 2.5 μ M required when Tm is absent). Second, the difference between binding of the phosphorylated and unphosphorylated C0–C2 is greater and the SDs of the lifetime changes are smaller. These two changes increase the robustness of screens as exemplified by the increases in Z' scores (Fig. 2 and Table 3). Finally, incorporating Tm into the initial screens is relatively simple and can

potentially reduce false positives, including drugs that affect binding to bare actin, but not when actin is decorated with Tm, as it would be in vivo. Using this technology, in the presence of Tm, identified drugs can be further tested to determine if their effect is through actin binding alone (by subsequently testing on bare actin) or if it is dependent on Tm. Also, this screening method sets the stage for future work using reconstituted thin filaments containing the Ca^{2+} -regulated troponin complex.

C0–C2 phosphorylation effects in TR-F and cosedimentation binding assays

Both TR-F and cosedimentation assays offer quantitative evaluation of actin binding. In addition to being high throughput and low manual effort, the TR-F assay has the added advantage of having a higher sensitivity to detect changes in binding due to phosphorylation. Differences in binding between phosphorylated and unphosphorylated C0–C2 are magnified in TR-F measurements as compared with cosedimentation (Table 1). On bare actin, the difference in K_d 's is 8 \times for TR-F and 1.5 \times for cosedimentation. On actin–Tm, the changes in K_d 's are 2.6 \times for TR-F and 2 \times for cosedimentation. Differences in the two assays may result from there being multiple binding sites on C0–C2 for multiple binding sites on actin (Orlova et al., 2011; Harris et al., 2016; Risi et al., 2018). PKA may affect a particular binding interaction that has a smaller consequence on C0–C2 remaining bound to actin than it has on C0–C2's influence on the lifetime of IAEDANS attached to actin's Cys-374. Additionally, we have previously demonstrated large phosphorylation effects on actin's structural dynamics that accompany small or no changes in binding as measured by cosedimentation (Bunch et al., 2019). These changes in dynamics likely arise from changes in binding sites, but an additional possibility is that actin's structural dynamics, in the presence of bound phosphorylated C0–C2, contributes to the lifetime changes of IAEDANS attached to actin's Cys-374. Finally, using C1–C2 fragments of rat cMyBP-C, changes in the activation state of native thin filaments due to phosphorylation of cMyBP-C were found to be greater than the effects on binding as measured by cosedimentation (Ponnam et al., 2019). Changes in binding sites and changes in dynamics or activation status are likely linked and either, or both, may explain the magnification of the differences we observe by TR-F. Whatever the mechanism explaining the increased difference measured by TR-F, it offers a different and complementary binding assay to be used in conjunction with cosedimentation and an improvement for screening purposes and scientific discovery.

C0–C2 mutation effects in TR-F and cosedimentation binding assays

We further validated the TR-F assay by testing its ability to probe cMyBP-C's actin-binding capacity when mutated to contain previously described HCM and Tm-binding mutants and deletion of the M-domain and C2.

M-C2 deletion

Complete removal of the M-domain and C2, in the C0–C1 protein, showed dramatic reduction in actin binding when tested

using TR-F (Fig. 4). This is consistent with earlier cosedimentation results by us (Bunch et al., 2019) and others (Shaffer et al., 2009) and confirmed with cosedimentation under our specific binding conditions (Fig. S7 and Table S1).

L352P

L352P displayed increased binding (Fig. 4), as has been previously demonstrated in mouse C1-C2 (Bezold et al., 2013).

E334K

The HCM mutant E334K displayed binding that was similar to WT measured by TR-F and slightly increased binding when measured by cosedimentation (Figs. 4 and S8). This result was surprising, as the homologous mutant in mouse (E330K) showed greatly reduced binding to actin when tested in a C1-C2 fragment (Bezold et al., 2013). Also, E330K in mouse hearts shortened the duration of ejection (van Dijk et al., 2018). Differences in buffer conditions may explain different results, though our testing of a wide range of buffers made only subtle differences in the binding of WT C0-C2. The presence of the C0 and Pro/Ala-rich linker in our proteins and/or species-specific sequence differences may be responsible for the different results we observed. That binding is different with C0 is supported by Risi et al. (2018), who found that the presence of C0 influences the mode of actin binding of C0-C1. Mutation of the homologous residue, E248K, in slow skeletal MyBP-C (*MYBPC1*) was found to increase interactions with myosin (Stavusis et al., 2019). Increased binding to myosin by mouse E330K in cMyBP-C might explain the shortened duration of ejection seen by van Dijk et al. (2018). It will be interesting to determine if this mutation in cMyBP-C alters interactions with myosin or if its phenotype is related to impairing the ubiquitin-proteasome system (Bahrudin et al., 2008).

R282W

The HCM mutation R282W inhibits phosphorylation of Ser284 and in conditions of submaximal phosphorylation results in increased actin binding by C0-C2. R282W is located in a PKA recognition sequence RRIS in the M-domain (Fig. 3). We predicted that it would reduce or eliminate phosphorylation of Ser284 by PKA. Mass spectrometry data suggest this is the case. When relatively high levels of PKA were used to maximally phosphorylate C0-C2, R282W had no significant effect on binding of phosphorylated C0-C2 to actin when compared with phosphorylated WT C0-C2 (Fig. 5 A and Table 2). Looking at the details of binding (Fig. 5 A), there is the suggestion that R282W reduces the effect of maximal phosphorylation. Unphosphorylated R282W appears to bind actin slightly less than WT, while phosphorylated R282W binds slightly more. This might indicate a reduced PKA effect (increased actin binding), as was predicted. As cMyBP-C is found in a range of PKA phosphorylation states, we used the TR-F assay to test a range of phosphorylation levels in WT and the R282W mutant. At intermediate levels of phosphorylation, we found a very significant difference in binding (Fig. 5; see also Fig. S5 for actin-Tm). C0-C2 binding was more inhibited by PKA treatment in WT than was R282W, which behaved more like unphosphorylated

protein. We conclude that the remaining three serines, when phosphorylated at high levels, are sufficient to reduce actin binding to a similar extent as when all four serines are phosphorylated. However, at reduced phosphorylation levels that we expect to be found in cardiac tissue, and especially in HCM (El-Armouche et al., 2007), there is a difference that results in R282W binding more strongly to actin. The TR-F multiwell plate assay greatly facilitated this testing of multiple phosphorylation levels to reveal a potential explanation of how R282W initiates or responds to HCM.

C1 Tm-binding region

The Tm-binding mutants changed a proposed Tm-binding region in C1 from RASK to either RRKK (adding positively charged amino acids) or EASE (reversing the charges from positive to negative). These mutants displayed, at physiologically relevant substoichiometric levels, increases and decreases in binding, respectively, to actin-Tm (Fig. 6 and Table 2). This is consistent with their effects on thin filament activation of myosin ATPase (Risi et al., 2018). Interestingly, they also show smaller, but significant, differences on bare actin (Fig. 6 and Table 2).

Testing of the TR-F assay with these mutations increases confidence in its ability to measure physiologically relevant changes in binding.

The TR-F assay can be modified to study other ABPs

Cys-374-IAEDANS-actin lifetime changes will likely be specific for the binding of a subset of ABPs. Though lifetime was affected by the binding of C0-C2 and by the phosphorylation or mutation status of C0-C2, not all ABPs will alter the lifetime of IAEDANS attached to Cys-374. A good example, provided here, is Tm. Tm complexed with actin had no detectable effect on IAEDANS lifetime. Lifetimes for both were in a range of 17.52–17.68 ns over three different preparations (see Table 3). For the TR-F-actin-binding assay to be useful for ABPs that do not interact with Cys-374, it will be necessary to label actin on different locations on its surface. Given the detailed understanding of actin's structure, and the ease of monitoring binding effects in the 384-well plate format, this is an attractive strategy to modify the current assay for other ABPs. Probes can be used to label actin at alternative sites that have been previously identified using muscle (Iwane et al., 2009) or yeast actin (Feng et al., 1997; Durer et al., 2012). Other strategies for labeling actin are available as well (Chen et al., 2012; Riedl et al., 2008).

Conclusion

The TR-F assay based on IAEDANS-labeled F-actin, in the 384-well plate format, has proven conducive to quick and easy optimization of conditions for the binding of cMyBP-C C0-C2 to actin and actin-Tm. Testing the binding of multiple mutant versions of C0-C2 and distinguishing between binding by phosphorylated and unphosphorylated states indicate it can be used as a high-throughput complementary assay to current cosedimentation assays that are much more labor intensive. We expect this assay to increase the rate of scientific discovery in understanding ABPs in health and disease. Z' score analysis indicates the assay is suitable for screening for drugs that

modulate cMyBP-C binding to actin or those that mimic the effects of phosphorylation on binding. In the absence of other screens with these specific capacities at the high-throughput level, the TR-F assay described here is a major advancement toward drug development based on cMyBP-C activity.

Acknowledgments

Richard L. Moss served as guest editor.

This work was supported by National Institutes of Health grants R00 HL122397 and R01 HL141564 (to B.A. Colson) and in part by a University of Arizona Sarver Heart Center Investigator Award (to B.A. Colson).

B.A. Colson filed a PCT patent application based on this work (patent pending, serial no. PCT/US21/14142). The other authors declare no competing financial interests.

Author contributions: B.A. Colson and T.A. Bunch designed the study and wrote the paper. T.A. Bunch, V.C. Lepak, and K.M. Bortz designed and purified recombinant proteins and DNA. T.A. Bunch and V.C. Lepak undertook purification of actin filaments for binding and TR-F assays. V.C. Lepak conducted sedimentation assays, and T.A. Bunch conducted TR-F assays. T.A. Bunch and B.A. Colson analyzed cosedimentation assays and fluorescence lifetime data. V.C. Lepak assisted with critical evaluation of the results and edited the manuscript. All authors critically evaluated and approved the final version of the manuscript.

Submitted: 17 July 2020

Accepted: 12 January 2021

References

Bahrudin, U., H. Morisaki, T. Morisaki, H. Ninomiya, K. Higaki, E. Nanba, O. Igawa, S. Takashima, E. Mizuta, J. Miake, et al. 2008. Ubiquitin-proteasome system impairment caused by a missense cardiac myosin-binding protein C mutation and associated with cardiac dysfunction in hypertrophic cardiomyopathy. *J. Mol. Biol.* 384:896–907. <https://doi.org/10.1016/j.jmb.2008.09.070>

Beausoleil, S.A., J. Villén, S.A. Gerber, J. Rush, and S.P. Gygi. 2006. A probability-based approach for high-throughput protein phosphorylation analysis and site localization. *Nat. Biotechnol.* 24:1285–1292. <https://doi.org/10.1038/nbt1240>

Bezold, K.L., J.F. Shaffer, J.K. Khosa, E.R. Hoye, and S.P. Harris. 2013. A gain-of-function mutation in the M-domain of cardiac myosin-binding protein-C increases binding to actin. *J. Biol. Chem.* 288:21496–21505. <https://doi.org/10.1074/jbc.M113.474346>

Bunch, T.A., V.C. Lepak, R.S. Kanassataga, and B.A. Colson. 2018. N-terminal extension in cardiac myosin-binding protein C regulates myofilament binding. *J. Mol. Cell. Cardiol.* 125:140–148. <https://doi.org/10.1016/j.yjmcc.2018.10.009>

Bunch, T.A., R.S. Kanassataga, V.C. Lepak, and B.A. Colson. 2019. Human cardiac myosin-binding protein C restricts actin structural dynamics in a cooperative and phosphorylation-sensitive manner. *J. Biol. Chem.* 294:16228–16240. <https://doi.org/10.1074/jbc.RA119.009543>

Chen, Q., S. Nag, and T.D. Pollard. 2012. Formins filter modified actin subunits during processive elongation. *J. Struct. Biol.* 177:32–39. <https://doi.org/10.1016/j.jsb.2011.10.005>

Copeland, O., S. Sadayappan, A.E. Messer, G.J. Steinen, J. van der Velden, and S.B. Marston. 2010. Analysis of cardiac myosin binding protein-C phosphorylation in human heart muscle. *J. Mol. Cell. Cardiol.* 49:1003–1011. <https://doi.org/10.1016/j.yjmcc.2010.09.007>

dos Remedios, C.G., and D.D. Thomas, editors. 2001. Molecular interactions of actin. Actin structure and actin-binding proteins. Springer Verlag, Berlin. <https://doi.org/10.1007/978-3-540-46560-7>

Durer, Z.A., D.S. Kudryashov, M.R. Sawaya, C. Altenbach, W. Hubbell, and E. Reisler. 2012. Structural states and dynamics of the D-loop in actin. *Biophys. J.* 103:930–939. <https://doi.org/10.1016/j.bpj.2012.07.030>

El-Armouche, A., L. Pohlmann, S. Schlossarek, J. Starbatty, Y.H. Yeh, S. Nattel, D. Dobrev, T. Eschenhagen, and L. Carrier. 2007. Decreased phosphorylation levels of cardiac myosin-binding protein-C in human and experimental heart failure. *J. Mol. Cell. Cardiol.* 43:223–229. <https://doi.org/10.1016/j.yjmcc.2007.05.003>

Feng, L., E. Kim, W.L. Lee, C.J. Miller, B. Kuang, E. Reisler, and P.A. Rubenstein. 1997. Fluorescence probing of yeast actin subdomain 3/4 hydrophobic loop 262–274. Actin-actin and actin-myosin interactions in actin filaments. *J. Biol. Chem.* 272:16829–16837. <https://doi.org/10.1074/jbc.272.27.16829>

Gruber, S.J., R.L. Cornea, J. Li, K.C. Peterson, T.M. Schaaf, G.D. Gillispie, R. Dahl, K.M. Zsebo, S.L. Robia, and D.D. Thomas. 2014. Discovery of enzyme modulators via high-throughput time-resolved FRET in living cells. *J. Biomol. Screen.* 19:215–222. <https://doi.org/10.1177/1087057113510740>

Gruen, M., H. Prinz, and M. Gautel. 1999. cAPK-phosphorylation controls the interaction of the regulatory domain of cardiac myosin binding protein C with myosin-S2 in an on-off fashion. *FEBS Lett.* 453:254–259. [https://doi.org/10.1016/S0014-5793\(99\)00727-9](https://doi.org/10.1016/S0014-5793(99)00727-9)

Harris, S.P., B. Bellknap, R.E. Van Sciver, H.D. White, and V.E. Galkin. 2016. C0 and C1 N-terminal Ig domains of myosin binding protein C exert different effects on thin filament activation. *Proc. Natl. Acad. Sci. USA.* 113:1558–1563. <https://doi.org/10.1073/pnas.1518891113>

Howarth, J.W., S. Ramisetty, K. Nolan, S. Sadayappan, and P.R. Rosevear. 2012. Structural insight into unique cardiac myosin-binding protein-C motif: a partially folded domain. *J. Biol. Chem.* 287:8254–8262. <https://doi.org/10.1074/jbc.M111.309591>

Ingles, J., J. Goldstein, C. Thaxton, C. Caleshu, E.W. Corty, S.B. Crowley, K. Dougherty, S.M. Harrison, J. McGlaughon, L.V. Milko, et al. 2019. Evaluating the Clinical Validity of Hypertrophic Cardiomyopathy Genes. *Circ. Genom. Precis. Med.* 12:e002460. <https://doi.org/10.1161/CIRCGEN.119.002460>

Iwane, A.H., M. Morimatsu, and T. Yanagida. 2009. Recombinant alpha-actin for specific fluorescent labeling. *Proc. Jpn. Acad., Ser. B, Phys. Biol. Sci.* 85:491–499. <https://doi.org/10.2183/pjab.85.491>

Jacques, A.M., O. Copeland, A.E. Messer, C.E. Gallon, K. King, W.J. McKenna, V.T. Tsang, and S.B. Marston. 2008. Myosin binding protein C phosphorylation in normal, hypertrophic and failing human heart muscle. *J. Mol. Cell. Cardiol.* 45:209–216. <https://doi.org/10.1016/j.yjmcc.2008.05.020>

Jia, W., J.F. Shaffer, S.P. Harris, and J.A. Leary. 2010. Identification of novel protein kinase A phosphorylation sites in the M-domain of human and murine cardiac myosin binding protein-C using mass spectrometry analysis. *J. Proteome Res.* 9:1843–1853. <https://doi.org/10.1021/pr901006h>

McConnell, M., L. Tal Grinspan, M.R. Williams, M.L. Lynn, B.A. Schwartz, O.Z. Fass, S.D. Schwartz, and J.C. Tardiff. 2017. Clinically Divergent Mutation Effects on the Structure and Function of the Human Cardiac Tropomyosin Overlap. *Biochemistry.* 56:3403–3413. <https://doi.org/10.1021/acs.biochem.7b00266>

Michie, K.A., A.H. Kwan, C.S. Tung, J.M. Guss, and J. Trewhella. 2016. A Highly Conserved Yet Flexible Linker Is Part of a Polymorphic Protein-Binding Domain in Myosin-Binding Protein C. *Structure.* 24:2000–2007. <https://doi.org/10.1016/j.str.2016.08.018>

Monteiro, P.B., R.C. Lataro, J.A. Ferro, and F.C. Reinach. 1994. Functional alpha-tropomyosin produced in Escherichia coli. A dipeptide extension can substitute the amino-terminal acetyl group. *J. Biol. Chem.* 269:10461–10466. [https://doi.org/10.1016/S0021-9258\(17\)34082-6](https://doi.org/10.1016/S0021-9258(17)34082-6)

Moss, R.L., D.P. Fitzsimons, and J.C. Ralphe. 2015. Cardiac MyBP-C regulates the rate and force of contraction in mammalian myocardium. *Circ. Res.* 116:183–192. <https://doi.org/10.1161/CIRCRESAHA.116.300561>

Mun, J.Y., M.J. Previs, H.Y. Yu, J. Gulick, L.S. Tobacman, S. Beck Previs, J. Robbins, D.M. Warshaw, and R. Craig. 2014. Myosin-binding protein C displaces tropomyosin to activate cardiac thin filaments and governs their speed by an independent mechanism. *Proc. Natl. Acad. Sci. USA.* 111:2170–2175. <https://doi.org/10.1073/pnas.1316001111>

Mun, J.Y., R.W. Kensler, S.P. Harris, and R. Craig. 2016. The cMyBP-C HCM variant L348P enhances thin filament activation through an increased shift in tropomyosin position. *J. Mol. Cell. Cardiol.* 91:141–147. <https://doi.org/10.1016/j.yjmcc.2015.12.014>

Muretta, J.M., A. Kyrychenko, A.S. Ladokhin, D.J. Kast, G.D. Gillispie, and D.D. Thomas. 2010. High-performance time-resolved fluorescence by direct

- waveform recording. *Rev. Sci. Instrum.* 81:103101. <https://doi.org/10.1063/1.3480647>
- O'Leary, T.S., J. Snyder, S. Sadayappan, S.M. Day, and M.J. Previs. 2019. MYBPC3 truncation mutations enhance actomyosin contractile mechanics in human hypertrophic cardiomyopathy. *J. Mol. Cell. Cardiol.* 127:165–173. <https://doi.org/10.1016/j.yjmcc.2018.12.003>
- Orlova, A., V.E. Galkin, C.M. Jeffries, E.H. Egelman, and J. Trewthella. 2011. The N-terminal domains of myosin binding protein C can bind polymorphically to F-actin. *J. Mol. Biol.* 412:379–386. <https://doi.org/10.1016/j.jmb.2011.07.056>
- Otterbein, L.R., P. Graceffa, and R. Dominguez. 2001. The crystal structure of uncomplexed actin in the ADP state. *Science.* 293:708–711. <https://doi.org/10.1126/science.1059700>
- Ponnam, S., I. Sevrieva, Y.B. Sun, M. Irving, and T. Kampourakis. 2019. Site-specific phosphorylation of myosin binding protein-C coordinates thin and thick filament activation in cardiac muscle. *Proc. Natl. Acad. Sci. USA.* 116:15485–15494. <https://doi.org/10.1073/pnas.1903033116>
- Riedl, J., A.H. Crevenna, K. Kessenbrock, J.H. Yu, D. Neukirchen, M. Bista, F. Bradke, D. Jenne, T.A. Holak, Z. Werb, et al. 2008. Lifeact: a versatile marker to visualize F-actin. *Nat. Methods.* 5:605–607. <https://doi.org/10.1038/nmeth.1220>
- Risi, C., B. Belknap, E. Forgacs-Lonart, S.P. Harris, G.F. Schröder, H.D. White, and V.E. Galkin. 2018. N-Terminal Domains of Cardiac Myosin Binding Protein C Cooperatively Activate the Thin Filament. *Structure.* 26:1604–1611.e4. <https://doi.org/10.1016/j.str.2018.08.007>
- Sadayappan, S., H. Osinska, R. Klevitsky, J.N. Lorenz, M. Sargent, J.D. Molkentin, C.E. Seidman, J.G. Seidman, and J. Robbins. 2006. Cardiac myosin binding protein C phosphorylation is cardioprotective. *Proc. Natl. Acad. Sci. USA.* 103:16918–16923. <https://doi.org/10.1073/pnas.0607069103>
- Schaaf, T.M., K.C. Peterson, B.D. Grant, P. Bawaskar, S. Yuen, J. Li, J.M. Muretta, G.D. Gillispie, and D.D. Thomas. 2017. High-Throughput Spectral and Lifetime-Based FRET Screening in Living Cells to Identify Small-Molecule Effectors of SERCA. *SLAS Discov.* 22:262–273.
- Schmidt, W.M., W. Lehman, and J.R. Moore. 2015. Direct observation of tropomyosin binding to actin filaments. *Cytoskeleton (Hoboken).* 72:292–303. <https://doi.org/10.1002/cm.21225>
- Shaffer, J.F., R.W. Kensler, and S.P. Harris. 2009. The myosin-binding protein C motif binds to F-actin in a phosphorylation-sensitive manner. *J. Biol. Chem.* 284:12318–12327. <https://doi.org/10.1074/jbc.M808850200>
- Stavusis, J., B. Lace, J. Schäfer, J. Geist, I. Inashkina, D. Kidere, S. Pajusalu, N.T. Wright, A. Saak, M. Weinhold, et al. 2019. Novel mutations in MYBPC1 are associated with myogenic tremor and mild myopathy. *Ann. Neurol.* 86:129–142. <https://doi.org/10.1002/ana.25494>
- van Dijk, S.J., K.L. Bezold, and S.P. Harris. 2014. Earning stripes: myosin binding protein-C interactions with actin. *Pflugers Arch.* 466:445–450. <https://doi.org/10.1007/s00424-013-1432-8>
- van Dijk, S.J., K.B. Kooiker, N.C. Napierski, K.D. Touma, S. Mazzalupo, and S.P. Harris. 2018. Point mutations in the tri-helix bundle of the M-domain of cardiac myosin binding protein-C influence systolic duration and delay cardiac relaxation. *J. Mol. Cell. Cardiol.* 119:116–124. <https://doi.org/10.1016/j.yjmcc.2018.05.001>
- von der Ecken J., M. Müller, W. Lehman, D.J. Manstein, P.A. Penczek, S. Raunser. 2015. Structure of the F-actin-tropomyosin complex. *Nature.* 519:114–117.
- Zhang, J.H., T.D. Chung, and K.R. Oldenburg. 1999. A Simple Statistical Parameter for Use in Evaluation and Validation of High Throughput Screening Assays. *J. Biomol. Screen.* 4:67–73. <https://doi.org/10.1177/108705719900400206>

Supplemental material

Results

Testing five fluorescent probes for suitability in TR-F-actin-binding assay

To find a suitable fluorescent dye for the TR-F assay, actin was labeled on its surface-exposed cysteine (Cys-374) with five different thiol-reactive dyes. Decays of fluorescence from labeled actin and actin in the presence of 5 μM and 20 μM CO-C2 fragment were analyzed using Eq. 1 (see Materials and methods). Changes in lifetime due to binding of unphosphorylated and phosphorylated (by PKA) CO-C2 were compared (Fig. S1). At both 1 μM and 5 μM actin (white bars in Fig. S1, A and B), the reduction in lifetime due to the binding of 5 and 20 μM CO-C2 (gray and black bars) was highly significant ($P < 0.000002$) for IAEDANS, IAANS, CPM, and FMAL. For IANBD, significant effects were observed at 1 μM - and 5 μM -labeled actin with 20 μM CO-C2 ($P < 0.000002$ and $P < 0.015$). 5 μM CO-C2 incubated with IANBD-actin (at 1 μM and 5 μM) showed a reduction in lifetime that trended to, but did not reach, significance ($P = 0.058$ and 0.162). Phosphorylation, known to reduce CO-C2 binding to F-actin, significantly reduced the effect on the lifetime changes; it reduced the reduction in lifetime. Comparison of unphosphorylated versus phosphorylated CO-C2 (Fig. S1, A and B, gray versus pink and black versus red) showed significant changes ($P < 0.05$) that were observed for all probes, though not at all actin and CO-C2 concentrations. For IAANS-, CPM-, and FMAL-labeled actin, the differences due to phosphorylation were significant at both actin and CO-C2 concentrations. For IAEDANS-labeled actin, the differences due to phosphorylation were significant for 1 μM actin with 5 and 20 μM CO-C2 and for 5 μM actin with 5 μM CO-C2, but not 5 μM actin with 20 μM CO-C2 ($P = 0.24$). Lack of significant differences due to phosphorylation at a high concentration (20 μM) of CO-C2 is not unexpected as phosphorylated CO-C2 “catches up” with nonphosphorylated CO-C2 at maximal binding (see binding curve in Fig. 1 A). 1 μM IANBD-labeled actin and 20 μM CO-C2 did show a significant difference upon phosphorylation of CO-C2 ($P = 0.024$). The other three conditions tested using IANBD-actin (1 μM IANBD-actin with 5 μM CO-C2, 5 μM IANBD-actin with 5 or 20 μM CO-C2) showed no significant differences.

Optimization of TR-F assay conditions

We chose to optimize the screen using IAEDANS-actin. Using 1 μM IAEDANS-labeled F-actin, we tested different pH and ionic conditions and T_m levels to determine their effects (Fig. S2).

Increasing pH increases the difference between actin and actin- T_m binding to CO-C2

Varying the pH of M-ABB between 6.8 and 8.0 subtly altered TR-F lifetime changes reported for binding to bare actin or actin decorated with T_m (Fig. S2 A). T_m itself did not significantly change the lifetime of the IAEDANS-labeled F-actin. Both lifetimes were ~ 17.60 ns (see actin alone and actin- T_m alone values in Table 3). In the presence of T_m , at pH 6.8, changes in TR-F due to unphosphorylated CO-C2 binding were greater than on bare actin ($P = 0.16, 0.53, \text{ and } 0.001$ for 1.25, 5, and 20 μM CO-C2, respectively). At higher pH (7.5 and 8.0), the differences between actin and actin- T_m upon binding to CO-C2 were more significant ($P < 0.04$ for all unphosphorylated CO-C2 concentrations).

NaCl reduces T_m effects

At pH 6.8, replacing 100 mM KCl with 100 mM NaCl decreased the effect of T_m on binding of CO-C2 when unphosphorylated ($P = 0.83, 0.12, \text{ and } 0.33$ for 1.25, 5, and 20 μM CO-C2, respectively; Fig. S2 A).

Increasing pH reduces effects of CO-C2 PKA phosphorylation on TR-F-measured binding

TR-F detection of binding to bare actin and actin- T_m was responsive to PKA phosphorylation of CO-C2 at the lower CO-C2 concentrations. The responsiveness was reduced as the pH was increased from 6.8 to 7.5 and 8.0 (Fig. S2 A). At pH 6.8 with 100 mM KCl, for actin plus 1.25 and 5 μM CO-C2 and actin- T_m plus 1.25 and 5 μM CO-C2, these differences were typically significant when comparing minus and plus PKA ($P = 0.036, 0.173, 0.01 \text{ and } 0.02$, respectively; average $P = 0.060$). Increasing the pH to 7.5 or 8.0 reduced the responsiveness to phosphorylation. At pH 7.5, the same comparisons of minus and plus PKA gave $P = 0.015, 0.649, 0.053, \text{ and } 0.003$ (average $P = 0.180$). At pH 8.0, the same comparisons of minus and plus PKA gave $P = 0.649, 0.224, 0.103, \text{ and } 0.004$ (average 0.245).

NaCl increases PKA phosphorylation effects

Replacing KCl with NaCl increased changes due to PKA treatment. At pH 6.8 with 100 mM NaCl, for actin plus 1.25 and 5 μM CO-C2 and actin- T_m plus 1.25 and 5 μM CO-C2, differences were all significant when comparing minus and plus PKA ($P = 0.039, 0.030, 0.00003, \text{ and } 0.06$; average $P = 0.032$).

To maintain the ability to detect the effects of T_m and PKA phosphorylation by TR-F, we chose to continue with M-ABB containing KCl at pH 6.8.

100 mM KCl increases detection of PKA phosphorylation

M-ABB at pH 6.8 with KCl was further tested for the effects of different KCl concentrations. A greater effect of phosphorylation on TR-F at 100 mM KCl was observed than at 50 or 25 mM KCl. At 1.25 μM and 5 μM C0-C2 (levels showing submaximal binding) the 100 mM KCl level resulted in the largest differences between phosphorylated and unphosphorylated C0-C2 binding (Fig. S2 B). These largest differences were observed at 1.25 μM C0-C2, where the lifetime change was reduced, upon phosphorylation, by 79% for actin and 61% for actin-Tm (compare light gray with light pink bars in Fig. S2 B). This difference is due mainly to a reduction in the binding of phosphorylated C0-C2 as the KCl concentration was increased.

Actin/Tm ratio of 3.5:1 displays significant Tm and PKA phosphorylation effects on TR-F lifetime changes

At pH 6.8 and 100 mM KCl, we compared the effect of different ratios of actin to Tm on the ability of TR-F to detect changes in the lifetime of IAEDANS-actin mediated by PKA phosphorylation of C0-C2 (Fig. S2 C). At 7:1 (actin/Tm), binding of C0-C2 was not significantly different than that seen with actin alone. Comparison of changes in lifetime between actin and 7:1 (actin/Tm) at three concentrations (0.325, 1.25, and 5 μM) of unphosphorylated C0-C2 gave average P values of 0.54, 0.85, and 0.27. When Tm was included at higher concentrations (5:1 and 3.5:1 actin/Tm), increases in the lifetime changes were observed. The P values for 5:1 actin/Tm compared with actin alone over the three concentrations of C0-C2 were 0.53, 0.09, and 0.44. For 3.5:1, the P values were 0.03, 0.03, and 0.29, as the lifetimes were reduced compared to those observed with actin alone. Therefore, increasing Tm to 5:1 or 3.5:1 increased the effects of C0-C2 on lifetime changes, presumably by increasing binding. At 5:1 and 3.5:1 actin/Tm, the greatest effects (changes in lifetimes) due to PKA phosphorylation were observed at 1.25 μM C0-C2 (dark gray versus dark pink bars; Fig. S2 C). At this concentration of C0-C2, the change in lifetime due to PKA phosphorylation was reduced 76% (from a lifetime change of 2.96% to 0.71%) at 5:1 actin/Tm and at 3.5:1, the reduction was 79% (from a lifetime change of 3.98% to 0.83%). To maintain the maximal effect of Tm, the 3.5:1 (actin/Tm) ratio was used in the subsequent experiments. Cosedimentation experiments confirmed that at this ratio, 3.5:1, Tm was in excess of the amount needed (7:1, actin/Tm) to decorate F-actin. Approximately half of the Tm cosedimented with the F-actin, and half remained in solution (Fig. S3).

Analysis of multiple factors affecting binding of C0-C2 to actin

In the main text, we validated the optimized TR-F assay's ability to detect changes in binding due to individual variables, including PKA phosphorylation, the presence of Tm on actin, and six different mutations in C0-C2. The TR-F-actin-binding assay in the multiwell format makes feasible the testing of multiple coincident variables as well. These tests were done at the same time as the individual tests, and the results are presented here. Binding curves were determined for the six mutant C0-C2 proteins to IAEDANS-actin and IAEDANS-actin-Tm, without and with phosphorylation (Figs. S4 and S6). The apparent K_d and B_{max} for the mutants with these variables included are given in Table S1. These curves, though commonly used for comparisons of cMyBP-C to actin, are dependent on maximal binding levels that are subject to artifacts. The maximal levels are also not found in vivo (see Discussion in the main text for a discussion of potential problems using K_d and B_{max} for comparisons). Therefore, we have compared the TR-F results for binding at specific substoichiometric concentrations of C0-C2. In most cases, these concentrations are 2.5 μM C0-C2 for actin and 1.25 μM C0-C2 for actin-Tm. They are same concentrations that showed the largest difference between phosphorylated and nonphosphorylated forms of WT C0-C2 (see main text), and they reflect conditions in vivo where C0-C2 would be found only one for every seven actin monomers. In cases where binding is enhanced by mutations (L352P and A216R/S217K), comparisons at lower concentrations were more informative. For comparisons of actin versus actin-Tm when C0-C2 was phosphorylated (and therefore showed reduced binding), comparisons at higher C0-C2 concentrations were most useful. Binding levels, as reported by TR-F, at specific C0-C2 concentrations used for comparison of different conditions in the following supplemental Results section are all taken from the binding curves and presented in Table S2 for all mutants. Finally, binding was assessed by cosedimentation for all the mutants at low (submaximal; 1.25 μM) and eightfold higher (10 μM , to demonstrate that 1.25 μM was indeed submaximal) concentrations. These too were conducted for actin and actin-Tm, unphosphorylated and phosphorylated, and can be found in Fig. S8. For C0-C2 and C0-C1, full cosedimentation binding curves were compared (Fig. S7).

C0-C1

C0-C1 binding to actin is increased by Tm. Though C0-C1 binding to actin is reduced compared to C0-C2 (see main text), its binding is increased by the presence of Tm. Comparing binding at 2.5 μM C0-C1, binding to actin-Tm was increased by 210% ($P < 0.05$). This is consistent with Tm binding to the C1 domain (Risi et al., 2018). As the motif (containing the PKA phosphorylation sites) is absent in C0-C1, PKA-treated C0-C1 was not done. Cosedimentation results under identical conditions show similar findings (Table S1 and Fig. S7).

L352P

L352P C0-C2 HCM mutation increased binding to actin as predicted (main text). The TR-F assay readily detected a 26% increase in binding of 1.25 μM C0-C2 L352P versus WT ($P < 0.00001$) to actin-Tm. When phosphorylated by PKA, the increases in binding of L352P to actin (at 2.5 μM C0-C2) and actin-Tm (at 1.25 μM C0-C2) were 218% ($P < 0.005$) and 204% ($P < 0.00001$), respectively,

relative to WT C0–C2. At the same concentrations, phosphorylation of L352P reduced its binding to actin, compared to unphosphorylated L352P, by 53% ($P < 0.0001$) and its binding to actin–Tm by 36% ($P < 0.0001$). The effect of Tm on the binding of L352P, either unphosphorylated or phosphorylated, was not significant. Cosedimentation measurement of L352P, at submaximal binding levels, to actin and actin–Tm showed qualitatively the same effects as reported by TR-F. Binding was increased by L352P in both the unphosphorylated and phosphorylated states to both actin and actin–Tm (all $>80\%$ and $P < 0.000001$).

E334K

E334K did not show significant changes in binding to actin at 2.5 μM (main text) or actin–Tm at 1.25 μM when compared with WT C0–C2. Comparing phosphorylated E334K and WT showed no significant differences in binding to actin or actin–Tm (Fig. S4). Phosphorylation of E334K reduced its binding to actin (at 2.5 μM) by 74% ($P < 0.0001$) and its binding to actin–Tm (at 1.25 μM) by 80% ($P < 0.0001$). Tm increased E334K's binding compared to actin alone by $\sim 300\%$ at 0.313 and 0.625 μM E334K ($P = 0.011$). For phosphorylated E334K at 2.5 μM , Tm increased binding by 200% ($P < 0.0001$). In cosedimentation measurements of E334K at 1.25 μM , binding to actin and actin–Tm was observed to be modestly increased (14% [$P < 0.02$] and 19% [$P < 0.0001$], respectively). No significant changes were observed with phosphorylated E334K.

R282W

R282W showed modest reductions in binding to actin when not phosphorylated (main text). On actin–Tm, R282W again showed a reduction in binding of 10% at 1.25 μM ($P < 0.01$) compared to WT. R282W reduced phosphorylation and increased binding, when treated with PKA, to actin (main text). The same reduced PKA effects (more binding and larger change in TR-F) were observed for binding to actin–Tm when R282W was treated with intermediate levels of PKA (0.5 and 1.5 ng PKA/ μg C0–C2; Fig. S5). At high levels of phosphorylation mediated by 7.5 ng PKA/ μg C0–C2, R282W binding to actin–Tm was the same as WT. As was the case for WT, maximal phosphorylation of R282W significantly reduced its binding to actin by 68% ($P < 0.0001$) and actin–Tm by 68% ($P < 0.0001$). Tm increased the binding of unphosphorylated R282W, at 1.25 μM , by 97% to actin ($P < 0.0001$) and phosphorylated R282W, at 2.5 μM , by 104% ($P < 0.005$). Cosedimentation showed similar levels of binding of R282W, compared to WT C0–C2, to actin and actin–Tm when unphosphorylated but increased binding to actin (39%, $P < 0.002$) and actin–Tm (48%, $P < 0.002$) when R282W was maximally phosphorylated.

RASK

RASK (amino acids 215–218, in C1 that interact with Tm) mutations were shown to reduce actin–Tm binding upon charge reversal (RASK>EASE) or enhance actin–Tm binding with added positively charged amino acids (RASK>RRKK; main text). Smaller changes in binding to bare actin were also observed (main text). These mutants compared to WT continued to show differences when phosphorylated.

EASE

RASK>EASE, when phosphorylated, showed 62% reduction compared to WT ($P < 0.00001$) in binding to actin–Tm, at 2.5 μM . On bare actin, phosphorylated RASK>EASE compared to WT showed a 43% reduction ($P < 0.03$). Phosphorylation further reduced binding of the EASE mutant, at 2.5 μM , to actin by 78% ($P < 0.00001$) and 56% on actin–Tm ($P < 0.001$). As mentioned in the main text, compared to actin alone Tm reduced binding of unphosphorylated RASK>EASE by 37% ($P < 0.03$). For phosphorylated RASK>EASE, Tm neither enhances nor reduces binding (Fig. S6). Cosedimentation assays showed RASK>EASE reduced binding to actin–Tm by 22% ($P < 0.00001$). No significant changes were observed in binding to actin or when EASE was phosphorylated.

RRKK

RASK>RRKK (at 1.25 μM), when phosphorylated, showed a 217% increase ($P < 0.00001$) in binding to actin–Tm when compared with WT. Phosphorylated RASK>RRKK compared to WT on bare actin showed no significant difference in binding. This illustrates the importance of the RASK sequence to Tm interactions over actin interactions. Phosphorylation reduced binding of the RRKK mutant, at 1.25 μM , to actin by 75% ($P < 0.00001$) and at 0.625 μM , to actin–Tm by 73% ($P < 0.00001$). Tm increased binding of unphosphorylated RASK>RRKK by almost 600% ($P < 0.000001$) over that seen for actin alone at 0.313 μM . For phosphorylated RASK>RRKK, Tm enhances binding by 274% ($P < 0.000001$) over that seen for actin alone at 2.5 μM . For comparison, Tm enhances binding of unphosphorylated WT (0.625 μM) by 105% ($P < 0.000001$) and for phosphorylated WT (2.5 μM) by 115% ($P < 0.000001$) over that seen for actin alone. Cosedimentation assays showed RASK>RRKK at 1.25 μM increased binding when it was unphosphorylated or phosphorylated. For unphosphorylated RASK>RRKK the increase over WT was 51% and for actin–Tm it was 61%. For phosphorylated RASK>RRKK the increase over WT was 65% and for actin–Tm it was 108% ($P < 0.0001$ for all of these comparisons).

Discussion

Optimization of the fluorescence lifetime-based actin-binding assay for C0-C2

Fluorescent probe choice

Based on our results testing multiple fluorescent probes, we concluded that, once the concentrations and conditions are optimized, any of the probes tested could likely be used in a screen based on TR-F to detect binding to actin. Also, most dyes would be capable of detecting differences in that binding that are dependent on phosphorylation of C0-C2. We chose to optimize the screen using IAEDANS-actin. IAEDANS-actin at 1 μM reported the largest change in lifetime upon binding to C0-C2 (6.6% with 20 μM C0-C2), and it displayed relatively small variability (low standard error values). Importantly, at 1 μM actin it showed very reproducible changes upon phosphorylation of C0-C2 (Fig. S1).

Assay pH and ionic conditions

Optimizing binding conditions has resulted in decreased K_d and increased B_{max} values compared to previous work (discussed in the main text Discussion). Much of the increase in binding and enhancement of differences upon phosphorylation appears to be due to lowering the pH of binding from pH 8 to 6.8 (Fig. S2 A). At the lower pH values, the change in lifetime seen with 5 μM C0-C2 is close to that seen at the high, near-saturation value, lifetime change caused by 20 μM C0-C2. At pH 6.8, utilizing KCl instead of NaCl (the salt used in our previous cosedimentation assays; Bunch et al., 2019) increased the difference between effects of C0-C2 binding to actin versus Tm and may to a small extent reduce the differences seen upon PKA phosphorylation. It is not clear how change in pH between pH 8 and pH 6.8 influences the binding we observe by both TR-F and cosedimentation. We utilized KCl in subsequent assays, as K^+ is the predominant electrolyte in muscle tissue and KCl had been utilized in experiments where F-actin was decorated with Tm (von der Ecken et al., 2015).

Ionic strength could influence binding, as F-actin carries a net negative charge and phosphorylation clearly affects the charge of the M-domain in C0-C2, making it more negative as well. As KCl was varied between 50 and 100 mM, we found very little difference in binding of unphosphorylated C0-C2 to actin or actin-Tm, especially at the lower C0-C2 concentrations. We did see a decrease in binding of phosphorylated C0-C2, at low concentrations, as KCl was increased, with the largest difference observed at 100 mM. We did not test higher KCl concentrations, as Tm interactions with actin are decreased above 75 mM (Schmidt et al., 2015). We speculate that in the absence of phosphorylation, the modest increase in ionic strength from 50 and 100 mM does not interfere with the positive interactions within domains of C0-C2 or between C0-C2 and actin. When these interactions are stressed by the presence of phosphorylated M-domains, the increase in KCl may be enough to weaken them by ionic shielding.

Optimization of the actin/Tm ratio in TR-F assays

To ensure that actin was fully decorated with Tm, we included it at levels twofold higher than the expected bound 7:1 actin/Tm ratio. If C0-C2 was able to bind to free Tm, there was the potential problem that increasing Tm to levels of 5:1 or 3.5:1 might result in free Tm binding to C0-C2, reducing C0-C2 binding to the actin-Tm complexes and thereby reducing binding effects we observe on actin. This was not a problem, as increasing the Tm concentration did not interfere with actin binding but rather increased binding (Fig. S2 C). Therefore, to promote Tm fully decorating actin, we used a 3.5:1 ratio. At this Tm level, we observed the largest differences in lifetime detected between unphosphorylated and phosphorylated C0-C2 (Fig. S2 C).

Combinatorial effects of phosphorylation, mutation, and Tm

C0-C2 binding to actin is influenced by a combination of variables, including C0-C2 phosphorylation, C0-C2 mutations, and the presence of Tm. Generation of binding curves for all combinations of these variables was readily accomplished using the TR-F assay but would have been challenging by cosedimentation assays.

We found that binding to actin and actin-Tm by all C0-C2 mutants and WT C0-C2 was sensitive to phosphorylation by PKA. Even mutations that increased binding, L352P and RASK>RRKK (A216R/S217K), did not remove this binding sensitivity to PKA phosphorylation. PKA effects on the L352P mutation have been previously observed in mouse C1-C2 proteins (L348P; Bezold et al., 2013). R282W shows altered sensitivity to PKA treatment in actin binding due to its elimination of phosphorylation at Ser-284, as discussed in the main text. This sensitivity of R282W to phosphorylation was similar when tested for binding to actin-Tm.

Tm enhanced the binding of WT and all mutants (phosphorylated or not) tested with the exception of L352P and the RASK>EASE (R215E/K218E). That L352P (phosphorylated or not) binding to actin was not enhanced by Tm suggests that the L352P mutation, in the tri-helix bundle of the motif, may position C0-C2 domains differently on actin such that its interactions with Tm are removed or altered. RASK>EASE (R215E/K218E) in C1 was designed to inhibit observed C1-Tm interactions. For unphosphorylated RASK>EASE, Tm actually decreases binding compared with bare actin (see Discussion in the main text). When RASK>EASE is phosphorylated, Tm had neither positive nor negative effects. Increases in binding due to Tm were greatest for RASK>RRKK (A216R/S217K), which introduced additional positively charged amino acids to the Tm-binding region of C1. This increase was observed for both unphosphorylated and phosphorylated RASK>RRKK, as predicted. The next largest change due to Tm presence was the E334K

mutation. Tm promoted a 300% increase in binding at 0.313 and 0.625 μ M C0-C2. By comparison, for WT C0-C2, Tm promoted a 40% and 105% at the same concentrations. This suggests that the Lys present in E334K may interact electrostatically with the negatively charged Tm. It is unclear where this residue (Glu) is located relative to actin or Tm in the WT C0-C2. The enhancement of actin-Tm binding due to E334K and removal of Tm effects by L352P may indicate a connection between the tri-helix bundle in the motif and Tm interactions, as both of these mutations are located in this tri-helix bundle (Fig. 3). This same mutation has been identified in the slow skeletal *MYBPC1* gene (E248K) and is associated with increased myosin binding (Stavusis et al., 2019). More work is needed to understand the functional consequences of E248K.

It is notable that both the negative Tm-binding mutation RASK>EASE (R215E/K218E) and the Tm enhancing mutation RASK>RRKK (A216R/S217K) also decrease and enhance binding to bare actin, though to a lesser degree. Therefore, we cannot attribute all of the effects of these mutations solely to their effects on Tm interactions.

TR-F and cosedimentation

More limited cosedimentation experiments conducted under the same conditions as TR-F generally show similar effects of phosphorylation, mutations, and the presence of Tm as TR-F, though there are some differences. Differences may be explained by cosedimentation measuring the amount of C0-C2 bound to F-actin, irrespective of the mode of binding, and TR-F measuring both the amount of binding and the mode of binding. For example, multiple interaction domains in both C0-C2 and actin have been observed and this can result in multiple domains of a single C0-C2 binding to actin in multiple ways. If a variable affects only low-affinity interactions and not the high-affinity interactions, then we could see no effect in cosedimentation (binding happens and is driven by high-affinity interactions) but could see an effect by TR-F (high-affinity binding happens, and the effect on the low-affinity site can alter how the entire C0-C2 is positioned on F-actin, thereby affecting the lifetime of the fluorescent probe at Cys-374).

As with TR-F, cosedimentation under the same conditions shows decreased binding of WT C0-C2 upon phosphorylation and increased binding due to the presence of Tm. The effect of phosphorylation is enhanced in the TR-F assay compared to the cosedimentation assay. This suggests a different effect on actin brought about by binding to phosphorylated C0-C2. This is consistent with our recently published work showing differential effects of phosphorylated C0-C2 binding to actin (Bunch et al., 2019). Cosedimentation, like TR-F, shows dramatically reduced binding to C0-C1 and increased binding with L352P. For E334K, cosedimentation shows small increases in binding to actin and actin-Tm, suggesting that our failure to see decreased binding by TR-F is real despite being at odds with data from mouse C1-C2 experiments (Bezold et al., 2013). R282W cosedimentation showed increased binding when maximally phosphorylated compared to WT as predicted for a reduction in phosphorylation at Ser-284. For TR-F, the results were slightly different. Maximal phosphorylation did not show significantly increased interactions. We had to use reduced (intermediate) levels of phosphorylation to see the effect. This might be explained by the change from Arg to Trp reducing the TR-F and thereby masking the effect of Ser-284 not being phosphorylated. This is indeed suggested by the observation that without phosphorylation, R282W shows reduced binding/interaction as measured by TR-F. For the charge reversal mutation RASK>EASE (R215E/K218E) in the Tm-binding region of C1, cosedimentation confirmed the main conclusion of TR-F that it reduced binding to actin-Tm. Interestingly, unlike TR-F, cosedimentation of this mutation did not detect reductions in binding to actin or when it was phosphorylated. We suspect that this mutation may alter subtle details of C0-C2 that do not result in loss of binding under those conditions. Cosedimentation and TR-F results were similar for the RASK>RRKK (A216R/S217K), increasing binding to actin-Tm, but also to actin alone when phosphorylated.

These results comparing TR-F and cosedimentation assays show that the TR-F assay provides a complementary assay for studying ABP (like C0-C2) -actin interactions. It is similar to cosedimentation in measuring binding but may also be sensitive to different types of binding.

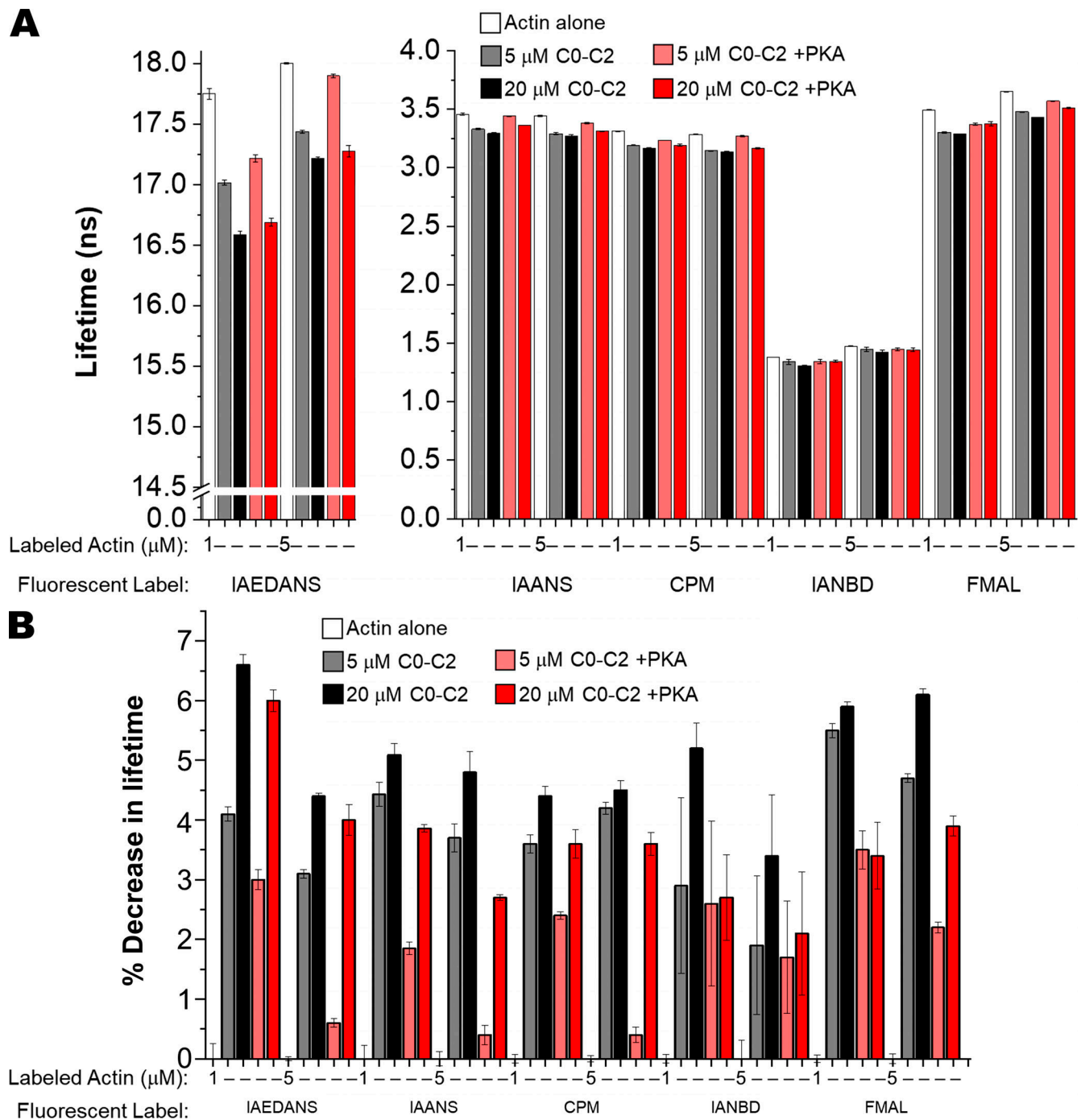


Figure S1. **Lifetime changes of five fluorescent dyes attached to actin at Cys-374 upon binding to C0-C2.** Either 1 or 5 μM of fluorescently labeled actin was mixed with 0, 5, or 20 μM unlabeled C0-C2. White bars indicate actin alone, gray/black bars indicate unphosphorylated C0-C2, and pink/red bars indicate phosphorylated C0-C2. (A) Fluorescence lifetime. (B) Relative reduction (% decrease) in lifetime compared with actin alone (see Materials and methods). Note that the actin alone (white bars) in B display only error bars, as the percent decrease in lifetime for actin alone relative to itself is 0. Significant differences were observed ($P < 0.000002$) for all probes comparing actin alone to actin plus C0-C2 (white bars versus gray, and white bars versus black) with two exceptions that trend to, but do not reach, significance in A or B: 1 μM IANBD-actin with 5 μM C0-C2 ($P = 0.06$) and 5 μM IANBD-actin with 5 μM C0-C2 ($P = 0.16$). For comparison of unphosphorylated versus phosphorylated C0-C2 (gray versus pink and black versus red), $P < 0.05$ for all probes and C0-C2 concentrations with four exceptions in A or B: 1 μM IANBD-actin 5 μM C0-C2 $P = 0.86$, 5 μM IANBD-actin 5 and 20 μM C0-C2 $P = 0.94$ and 0.40 , and 5 μM IAEDANS-actin 20 μM C0-C2 $P = 0.24$. Data are provided as mean \pm SE ($n > 4$).

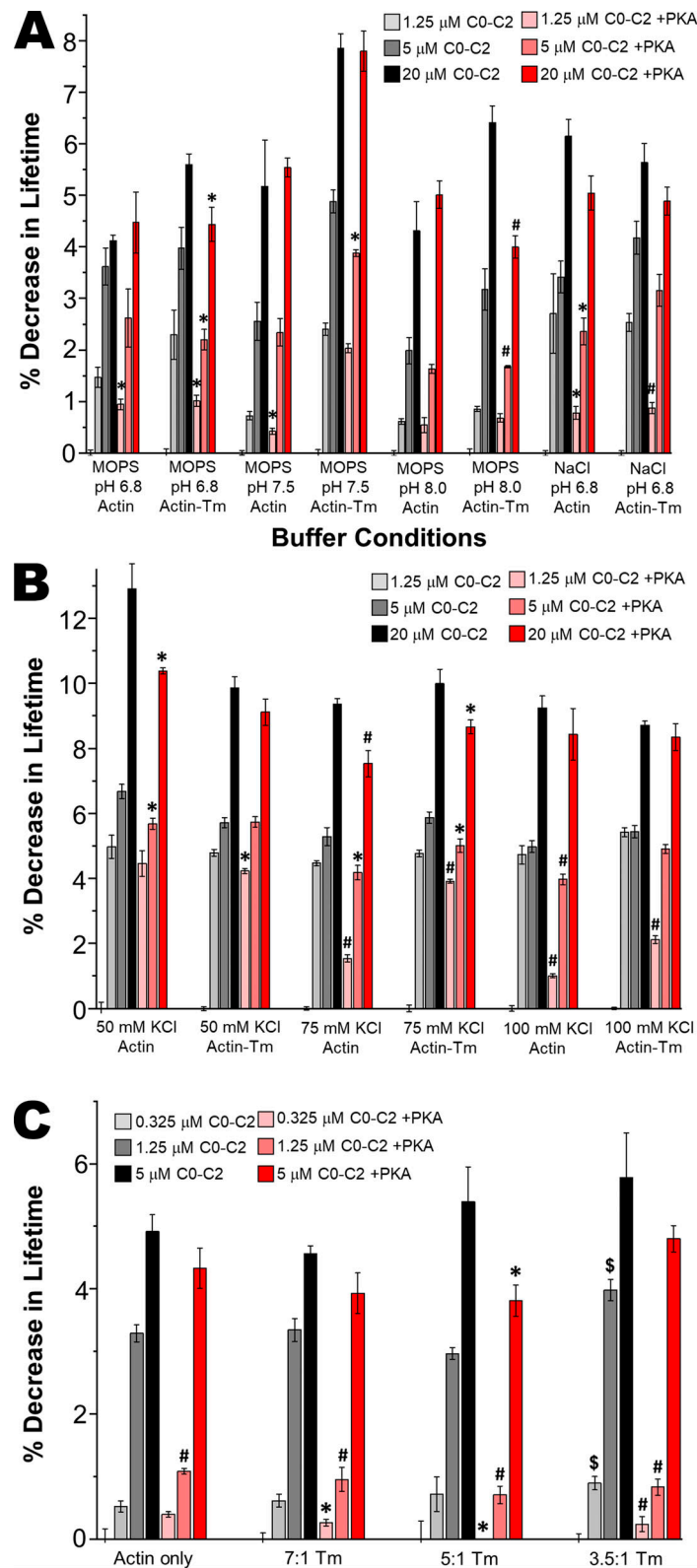


Figure S2. **Buffer conditions optimization of the TR-F assay for C0-C2 binding to IAEDANS-actin and IAEDANS-actin-Tm.** Reduction in lifetimes (% decrease) for either 1 μ M IAEDANS-labeled actin or actin-Tm binding to the indicated concentrations of C0-C2 that was not phosphorylated (gray and black) or phosphorylated by PKA (+PKA, pink and red). Note the first bar left of the six colored bars in each group shows 0% decrease in lifetime with baseline error bars for actin, or actin-Tm, alone (i.e., 0% decrease relative to itself). **(A)** Binding buffers at varying pH and either 100 mM KCl or NaCl. **(B)** Three concentrations of KCl in binding buffer. **(C)** Different ratios of actin/Tm. In C, for unphosphorylated C0-C2, significant differences comparing actin alone to actin/Tm are indicated ($\$$, $P < 0.05$). In A-C, significant differences between minus and plus PKA are indicated (*, $P < 0.05$; #, $P < 0.005$). Data are provided as mean \pm SE ($n > 4$).

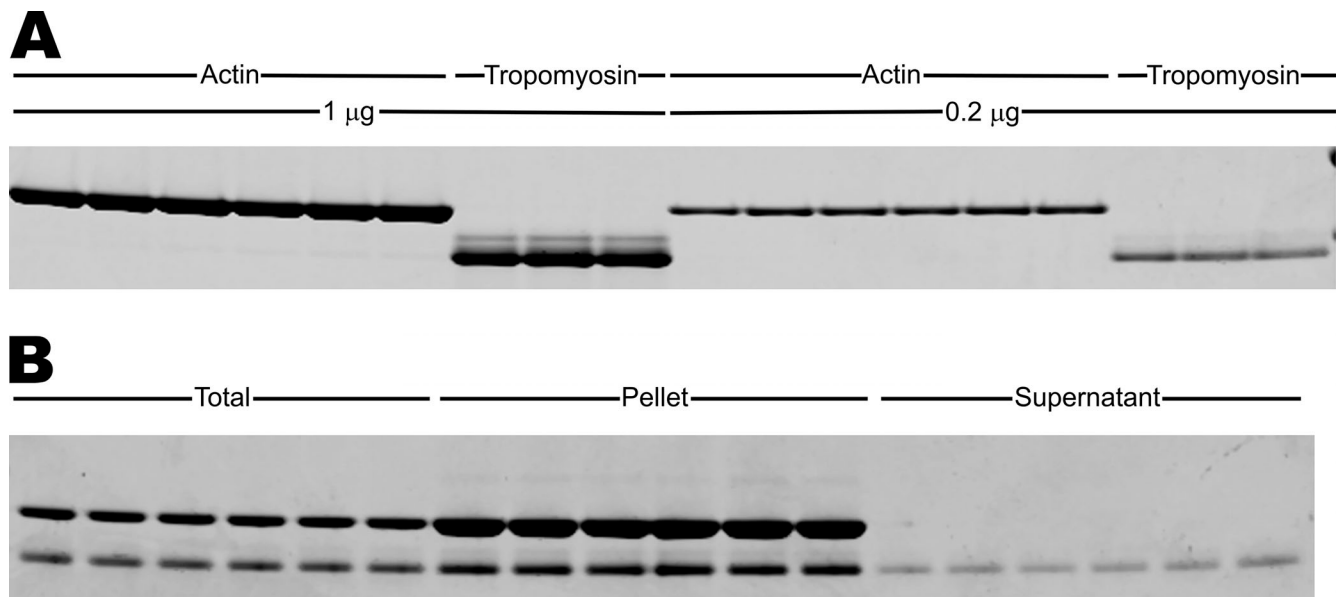


Figure S3. **Actin/Tm ratios.** (A) Relative staining intensity of actin and Tm in SDS-PAGE gels stained with Coomassie blue was determined. 1 µg actin from two separate preps (lanes 1–6) and 1 µg Tm (lanes 7–9) were compared as were 0.2 µg actin (lanes 10–15) and 0.2 µg Tm (lanes 16–18). The concentrations of actin and Tm were determined using their extinction coefficients. For actin, absorbance at 290 nm 0.1% (1 g/liter) was 0.63. For Tm absorbance at 280 nm 0.1% (1 g/liter) was 0.274. The average actin/Tm staining intensity ratio was 1.55. (B) Mixtures of 3.5:1 actin/Tm were made (total, first six lanes). Following centrifugation (TLA 100 rotor, 100,000 rpm, 30 min, 4°C) actin and bound (cosedimenting) Tm in the pellet were examined (pellet, lanes 7–12). Supernatant (unbound Tm) was also examined (supernatant, lanes 13–18). The relative intensities of the actin and Tm bands was 3:1 for the Total and 7.5:1 for the Pellet following correction for staining differences determined in A and differences in molecular weights (actin, 42,000 D; Tm dimer, 65,300 D). Total and Supernatant can be directly compared as the same volume was examined for each. 40% of the input Tm remained unbound indicating that there was excess Tm in the mixture. All of the actin was found in the pellet.

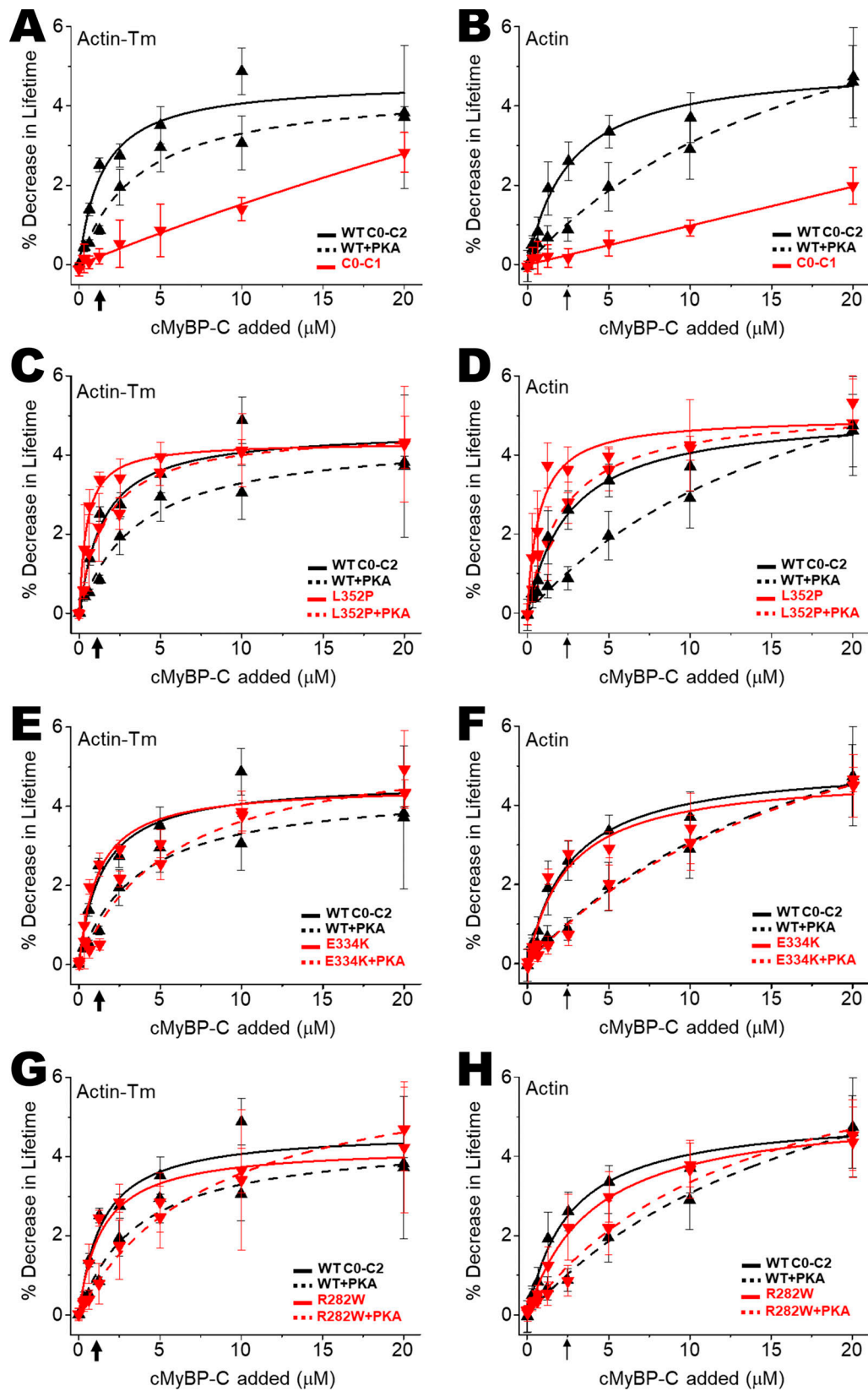


Figure S4. **TR-F IAEDANS-actin-Tm and IAEDANS-actin-binding curves for C0-C2 mutants.** TR-F measurements of the effects of mutant C0-C2 on the reduction (percent decrease) in lifetimes are plotted for increasing concentration without (solid red lines) and with PKA treatment (dotted red lines). For comparison, curves for WT C0-C2 are included in each graph (black lines). **(A)** C0-C1/actin-Tm. **(B)** C0-C1/actin. **(C)** L352P/actin-Tm. **(D)** L352P/actin. **(E)** E334K/actin-Tm. **(F)** E334K/actin. **(G)** R282W/actin-Tm. **(H)** R282W/actin. Arrows indicate the C0-C2 concentrations to be used in future screens (thick arrows, 1.25 μ M for actin-Tm in A, C, E, and G; thin arrows, 2.5 μ M for actin alone in B, D, F, and H). Data are provided as mean \pm SE ($n > 4$).

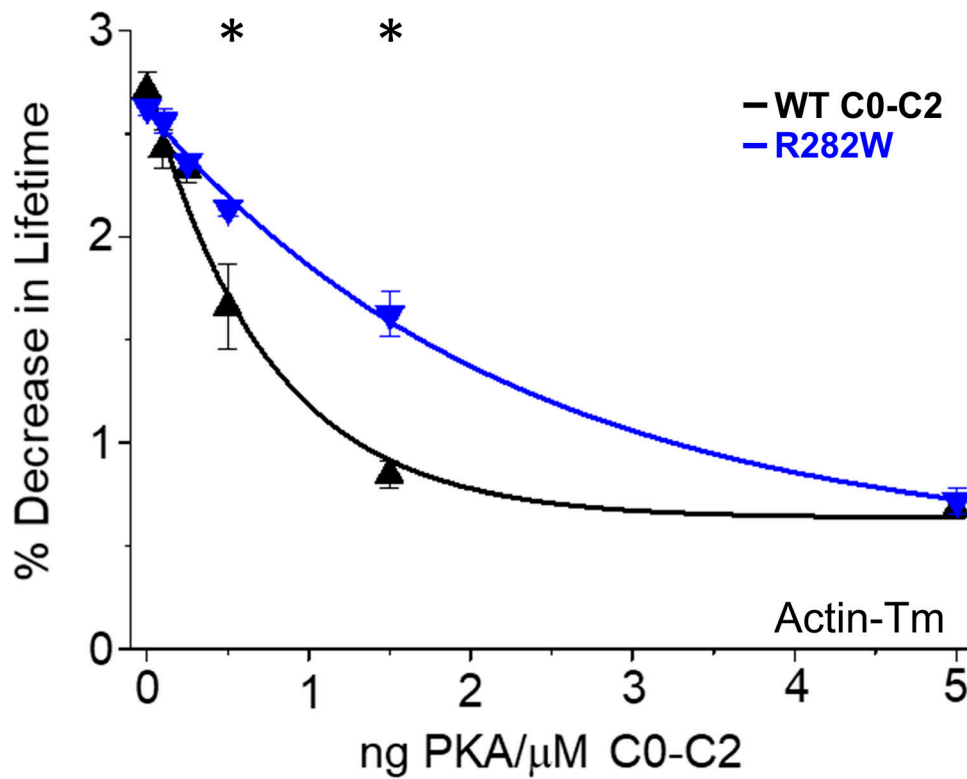


Figure S5. **Effects of R282W HCM mutant on phosphorylation-modulated binding to actin-Tm at submaximal phosphorylation by PKA.** Effects of HCM mutant R282W on C0-C2 phosphorylation were tested over a range (0–5 ng PKA/ μ g C0-C2) of PKA levels. WT and R282W effects on IAEDANS-actin-Tm lifetime change (percent decrease) as a function of PKA concentration. At intermediate phosphorylation levels (0.5 and 1.5 ng PKA/ μ M C0-C2), binding to actin or actin-Tm detected by TR-F is significantly increased in R282W (*, $P < 0.003$). Data are provided as mean \pm SE ($n > 4$).

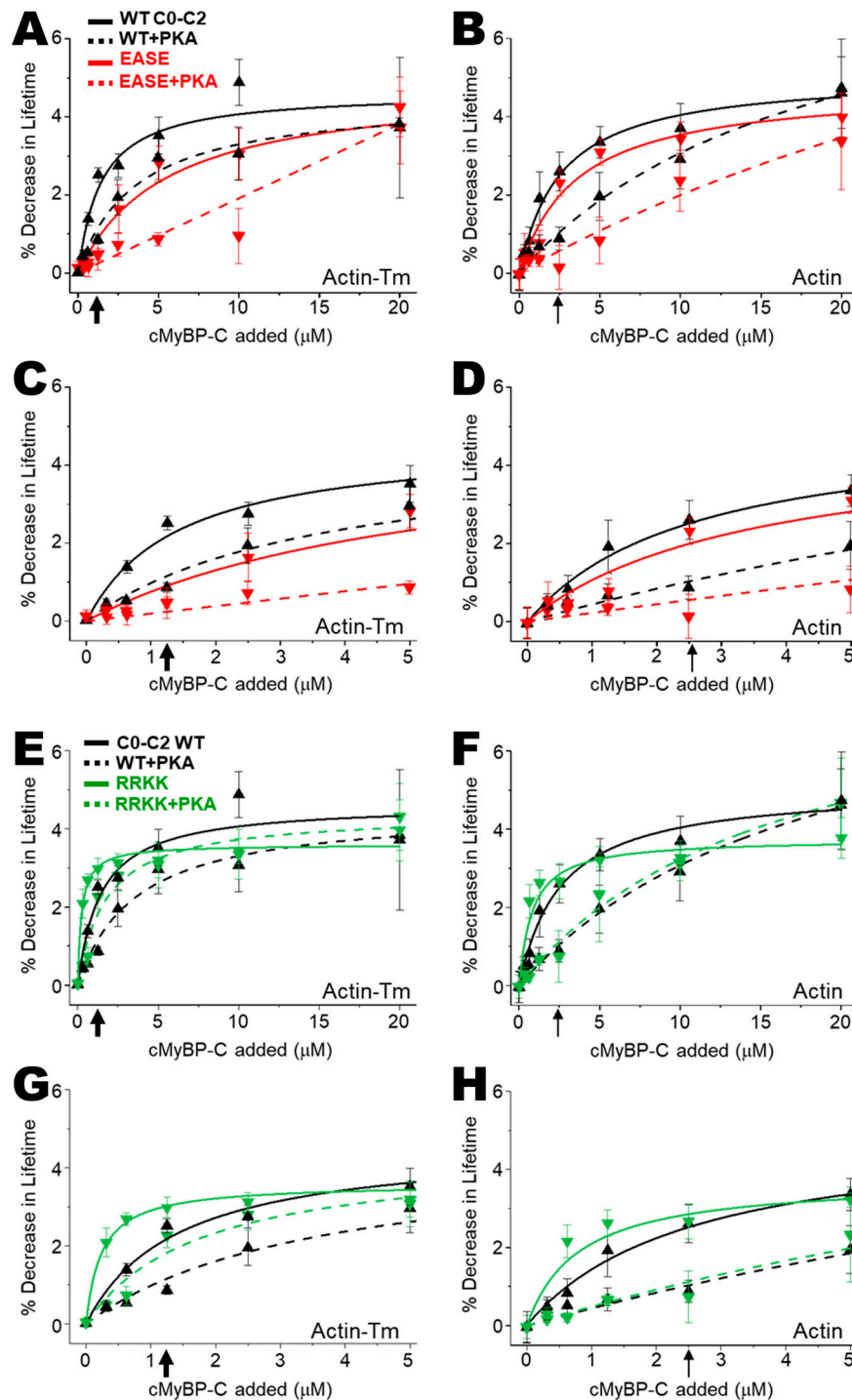


Figure S6. **Effects of Tm-binding mutants on phosphorylation-dependent binding to actin-Tm and actin.** Effects of Tm-binding mutants C0-C2 on actin-Tm and actin TR-F were tested with and without PKA treatment. Tm-binding mutants reverse charges (EASE; R215E/K218E) or introduce additional positive charges (RRKK; A216R/S217K) in the Tm-binding loop 215–218, RASK, of C0-C2. For comparison, curves for WT C0-C2 are included in each graph. **(A)** WT (black lines) and R215E/K218E (EASE in red) effects on IAEDANS-actin-Tm for unphosphorylated (solid lines) and phosphorylated (+PKA, dotted lines) C0-C2 from 0 to 20 μM cMyBP-C added. **(B)** Same conditions as A, except that IAEDANS-actin was used. **(C and D)** Zooming in on the lower concentrations (0 to 5 μM) cMyBP-C added in A and B. **(E-H)** The same conditions as A-D above but comparing WT (black lines) and A216R/S217K (RRKK in green). For the unphosphorylated Tm-binding mutant (charge reversal-EASE), apparent K_d changes trended toward significant ($P = 0.11$) for actin-Tm, but not for actin alone. The phosphorylated mutant did not fit well to a quadratic binding equation for either actin or actin-Tm (but did fit to a linear equation). For the unphosphorylated positive Tm-binding mutant (additional positive charges, RRKK) apparent K_d changes were significant ($P < 0.05$) for binding to both actin and actin-Tm. For phosphorylated RRKK binding, changes in K_d did not reach significance. Refer to Table S1 for statistical analysis of fitted binding properties for curves. See Table S2 for comparisons of binding at specific substoichiometric C0-C2 concentrations discussed in supplemental Results. Arrows indicate the C0-C2 concentrations to be used in future screens (thick arrows, 1.25 μM for actin-Tm in A, C, E, and G; thin arrows, 2.5 μM for actin alone in B, D, F, and H). Data are provided as mean \pm SE ($n > 4$).

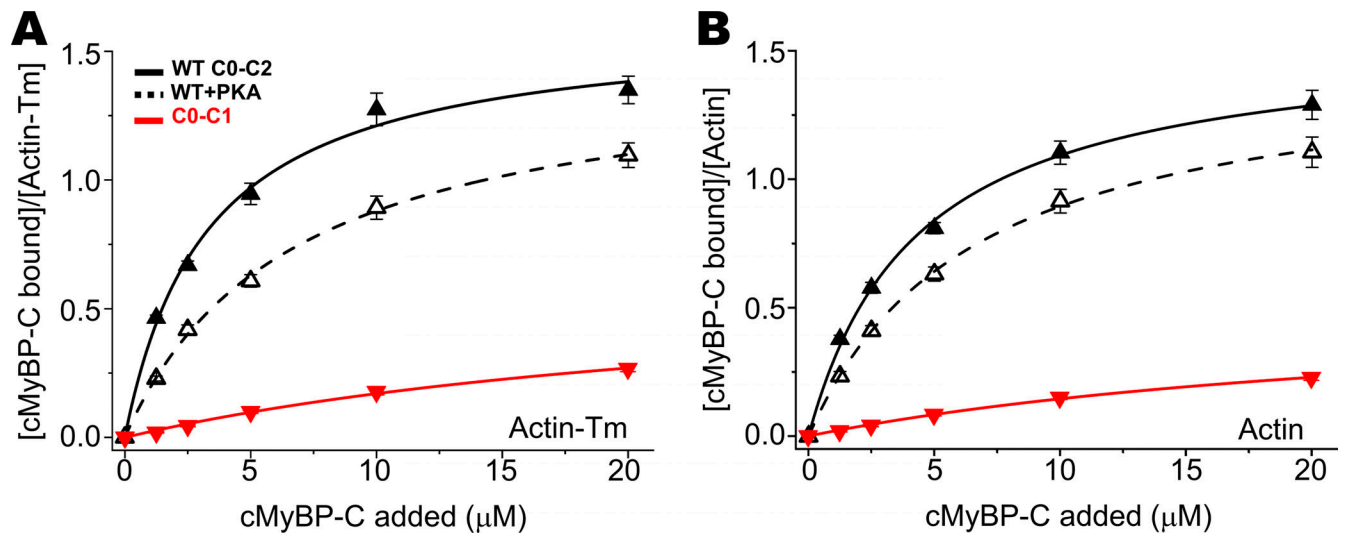


Figure S7. **Cosedimentation assays for C0-C1 binding to actin-Tm and actin.** C0-C1 (red lines) was assayed and unphosphorylated C0-C2 (solid lines), and phosphorylated C0-C2 (dotted lines) are shown for reference. **(A)** Cosedimentation using actin-Tm. **(B)** Cosedimentation using actin. Cosedimentation using actin-Tm or actin was also measured at 40 μM C0-C1, and this was used for determination of K_d and B_{max} for C0-C1 curves (Table S1). Data are provided as mean \pm SE ($n > 4$).

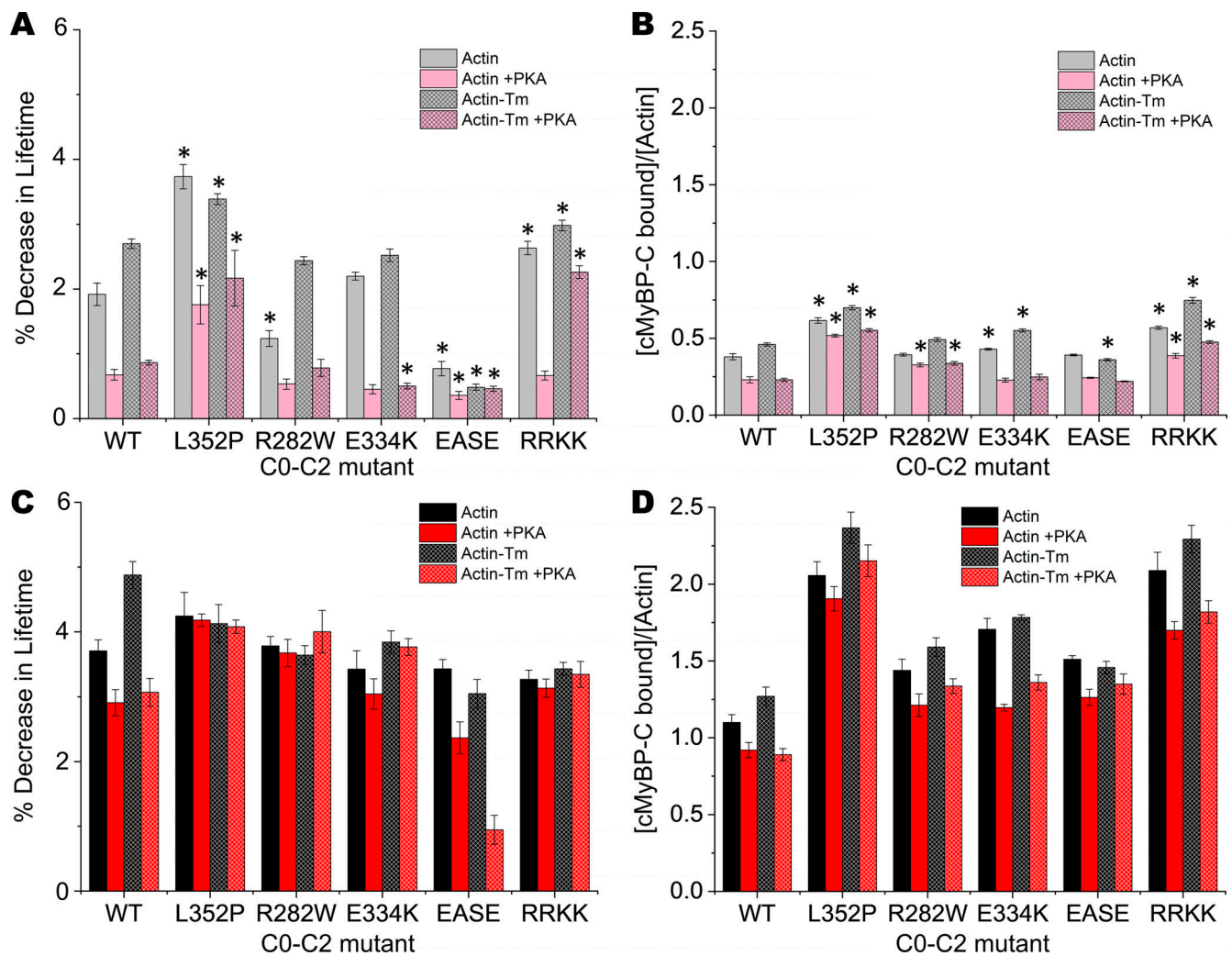


Figure S8. **Comparison of TR-F and cosedimentation actin-binding assays for C0-C2 mutants.** Unphosphorylated and phosphorylated WT and five mutants of C0-C2 were assayed using IAEDANS-actin or IAEDANS-actin-Tm. **(A)** TR-F using 1.25 μM C0-C2. **(B)** Cosedimentation using 1.25 μM C0-C2. **(C)** TR-F using 10 μM C0-C2. **(D)** Cosedimentation using 10 μM C0-C2. *, $P < 0.05$ for comparisons with WT under the same conditions at substoichiometric binding levels (1.25 μM C0-C2, A and B). In A and B, reduction in binding due to phosphorylation was significant ($P < 0.005$) in all cases with the exception of EASE C0-C2 binding to actin-Tm measured by TR-F. Data are provided as mean \pm SE ($n > 4$).

Tables S1, S2, S3, and S4 are provided online. Table S1 lists TR-F and cosedimentation binding parameters of WT and mutant MyBP-C/actin and actin-Tm. Table S2 lists change in IAEDANS lifetime for IAEDANS-actin and IAEDANS-actin-Tm upon substoichiometric binding of C0-C2 and C0-C1. Table S3 lists WT and R282W C0-C2 phosphorylated peptides. Table S4 lists peak intensity ratios for WT and R282W PKA phosphorylated/unphosphorylated peptides.